Phosphorus recovery from anaerobic membrane bioreactor (AnMBR) permeate by chemical coagulation and bioelectrochemical processes

by

Evan Heronemus

B.S., Kansas State University, 2015

A THESIS

submitted in partial fulfillment of the requirements for the degree

MASTER OF SCIENCE

Department of Civil Engineering
Carl R. Ice College of Engineering

KANSAS STATE UNIVERSITY
Manhattan, Kansas

2021

Approved by:

Major Professor
Dr. Prathap Parameswaran

Copyright

Abstract

As the world's population continues to increase, demand for natural resources will continue to grow, especially those needed for the production of food, energy, and water. Dwindling resources have already began pushing society towards a circular economy model, as supply chain disruptions and price instability of these limited resources creates a need to generate more raw materials from waste products. Phosphorus is one of these critical raw materials being depleted, which is mined for approximately 20 million tons each year. It is unclear how long these phosphate reserves will last, but it is estimated that demand could outpace supply this century, possibly by 2035. Anaerobic membrane bioreactors (AnMBRs) represent an emerging environmental biotechnology platform with the potential to simultaneously recover water, energy, as well as nutrients from a variety of different concentrated wastewaters, recycling the waste as raw materials into the circular economy. While AnMBRs keep the nutrients in a more easily recoverable form in the liquid stream, there is limited work demonstrating nutrient recovery paired with an AnMBR. This study focused on capturing the phosphorus present in the permeate from the AnMBR using conventional chemical coagulation-flocculation-sedimentation processes, further aided by emerging platforms such as bioelectrochemical systems for further polishing of the effluent and enhancing the nutrient product quality. This research was accomplished through four objectives. Objective 1 sought to evaluate performance of coagulation-flocculation-sedimentation systems for the simultaneous removal of phosphorus and sulfide from wastewater permeate after treatment through an anaerobic membrane bioreactor (AnMBR). Iron addition was found to effectively remove phosphate at an efficiency of over 90% in municipal wastewater with a sulfide removal of over 99% when the system was continuously operated, the findings from which were published in a peer reviewed journal. Calcium addition showed high phosphate removal with no significant sulfide removal, but long-

term continuous pilot scale data is still pending future work. Objective 2 aimed to assess the efficiency of iron phosphate recovery form wastewater and its potential as a fertilizer, and it was found that the recovered nutrient product acted as a phosphorus sink, giving it certain applications, but making it an ineffective fertilizer product. These findings were also published in a peer review journal. Objective 3 focused on tailored chemical addition of calcium to form the most calcium phosphate product that is most plant available. pH control was found to be important for producing a better product. Further removal will still be required after coagulation to meet discharge standards for swine wastewater, and capacitive deionization has the potential to achieve this, but future work outside the scope of this thesis is needed. However objective 4 aimed to provide preliminary steps for this process, by comparing the Coulombic recovery from acetate-fed and glucose-fed microbial electrochemical systems to determine the feasibility of directly feeding wastewater for capacitive deionization of phosphate. These experiments found methane to be a substantial electron sink at the anode, limiting the Coulombic efficiency of reactors with glucose as the substrate.

Table of Contents

List of Figures

List of Tables

Acknowledgements

I would first like to acknowledge the sources of funding for this research, including the United States Department of Agriculture (USDA)'s National Institute for Food and Agriculture (NIFA), the Department of Defense Environmental Security Program, the Kansas Agricultural Experiment Station, the Global Food System (GFS) program, the Kansas National Science Foundation EPSCoR (Established Program to Support Competitive Research), the NSF National Research Traineeship (NRT), the NSF Signals in the Soils (SiTS) program, and the Kansas State University Civil Engineering Department.

I would then like to thank Cody Delaney for his assistance in the labs and work preparing materials for the microbial electrolysis cells used in this research. I also want to thank the undergraduate students, past and present, who assisted with the experiments and made this research possible: Bernadette Drouhard, Megan Lehman, Jack Dillavou, and Madison King. I want to thank the following graduate students: Kahao Lim, Christopher Chiu, Arvind Kannan, Priyasha Fernando, Emily Randig, and Niloufar Fattahi for their help with the research, but mostly for their mentorship and encouragement. I also want to extend a special thanks to Kasuni Gamage, who co-authored the paper that forms Chapter 2 in this study.

Finally, I want to thank Dr. Prathap Parameswaran for his mentorship and expertise throughout my master's program, as well as my committee members, Dr. Jeongdae Im and Dr. Ganga Hettiarachchi, for their insights and support.

Chapter 1 - Introduction

1.1 Literature Review

As the world's population continues to increase, demand for natural resources will continue to grow, especially those needed for the production of food, energy, and water. Dwindling resources have already began pushing industry towards a circular economy model, as supply chain disruptions and price instability of these limited resources creates a need to generate more raw materials from more sustainable resources including waste products (Robles et al., 2020). Phosphorus is one of these critical raw materials being depleted, which is mined for approximately 20 million tons from phosphorus rock supplies in just a small number of countries, with Morocco holding up to 70% of these reserves (Cordell et al., 2011; Mayer et al., 2016). It is unclear how long these reserves will last, but it is estimated that demand could outpace supply within this century, possibly by 2035 (Cordell et al., 2011; Cordell et al., 2009; Cordell & White, 2013; Mayer et al., 2016).

There is increased focus on wastewater as part of this circular economy (Robles et al., 2020; Roychand et al., 2020), as wastewater contains nutrients (phosphorus and nitrogen) that can be recovered for fertilizer production, water that can be reused, and energy potential that can be harnessed from the organic matter (Robles et al., 2020). Many treatment plants are beginning to brand themselves as Water Resource Recovery Facilities (WRRFs) to align themselves with this theme and to accomplish it. Swine waste, as wastewater or manure, also has great potential to epitomize the circular economy concept. The organic and nutrient concentrations of swine wastewater are much higher than municipal wastewater, with a chemical oxygen demand (COD) that can be upwards of 10,000 mg/L and phosphorus and nitrogen concentrations that can be as high as 250 mg/L P and 1200 mg/L N (H.-H. Cheng et al., 2020). As this is about 10 times the

strength of municipal wastewater (Henze et al., 2008), there is even greater potential for pollution, but also greater potential energy recovery through biogas production from anaerobic processes and potential nutrient sequestration rather than its removal (H.-H. Cheng et al., 2020; Meinen et al., 2014).

Traditionally, wastewater treatment has focused on physical and biological processes that remove solids and organics from the waste to prevent pollution and oxygen depletion in the water bodies into which they are discharged. In more recent times, wastewater treatment has been additionally required to provide nutrient removal as well, as effluent nitrogen and phosphorus effluent limits have become stricter to attempt to reduce eutrophication leading to harmful algal blooms. At the same time, swine waste from small and large Confined Animal Feeding Operations (CAFOs) is rarely treated. Typically, it is stored in an anaerobic lagoon on site resulting in greenhouse gas emissions and the resulting stabilized sediments is land applied once (Nelson et al., 2003), while it is sparingly anaerobically digested (Meinen et al., 2014). Point and non-point discharge of nitrogen and phosphorus from wastewater effluent and runoff from agricultural and livestock operations causes eutrophication, resulting in hypoxic dead zones in freshwater aquatic ecosystems around the world, and may be one of the several factors that causes major annual outbreaks such as the one in Lake Erie and the Gulf of Mexico (Mayer et al., 2016; Robert J Diaz & Rutger Rosenberg, 2008). Freshwater eutrophication is estimated to produce economic damages of over $2.2 billion annually in the United States (Dodds et al., 2009; Mayer et al., 2016). In freshwater ecosystems, phosphorus is more critical to causing pollution, as it is often the limiting nutrient (David W Schindler et al., 2008). Biological nutrient removal (BNR) systems remove nitrogen and phosphorus together from municipal wastewater and produce a clean effluent that meets stringent total nitrogen and phosphorus discharge regulations, to produce effluent standards below 5 mg/L

as N and 0.5 mg/L as P (Bashar et al., 2018). However, beneficial recovery of these valuable nutrients has limited success in BNR systems, as the nitrogen is transformed to nitrogen gas and phosphorus remains trapped in the settled BNR sludge, with biosolids land application being the dominant reuse option (Tchobanoglous et al., 2014). There are several options available for a more effective recovery of phosphorus from municipal or agricultural wastewaters, apart from removal. The research carried out as part of this thesis will focus on chemical coagulation and flocculation processes, along with bioelectrochemical systems for further polishing, but membrane-based and photosynthetic-based processes are also being widely explored (Robles et al., 2020).

1.1.1 Chemical Precipitation Processes

Precipitation of struvite ($MgNH_4PO_4$ or KNH_4PO_4) is a popular means to achieve simultaneous recovery of phosphorus and nitrogen as phosphate and ammonia in the form of a slow-release fertilizer (Sengupta et al., 2015). The centrate from anaerobic digestion is an ideal environment for struvite to form, and chemicals such as magnesium chloride, hydroxide, or oxide are added to initiate and complete the precipitation reaction, while pH and temperature are carefully controlled to enable crystallization (Tchobanoglous et al., 2014; Pastor et al., 2010). There is an interest in more efficient slow-release fertilizers (Robles et al., 2020), as only 16% of phosphorus applied as fertilizer makes it to the end of food production (Mayer et al., 2016) The market for these slow-release fertilizers has allowed for several companies to develop various patented processes for struvite precipitation and crystallization, such as the Pearl, AirPrex, PHOSPHAQ, Phosnix, and Crystalactor processes, primarily working with municipal treatment plants to implement these processes and sell the products (Tchobanoglous et al., 2014; Giesen, 2009). Recovery of struvite has shown that the sale of phosphate-based products recovered from wastewater may not be economically feasible right now, especially with the current pricing of mineral fertilizers, but these

companies that produce struvite turn a profit by marketing themselves as providing valuable services, removing phosphorus in order to meet discharge regulations and assisting with research and technology development, along with the slightly less quality wastewater derived product, struvite (Mayer et al., 2016; Otoo et al., 2015). This is a good example of the circular economy in action.

However, struvite has several notable shortcomings. Its phosphorus recovery efficiency is relatively low (10-50% P sequestration efficiency) and is typically possible only in municipal wastewater treatment plants with enhanced biological phosphorus removal (EBPR), where process parameters can be carefully maintained (Ewert et al., 2014; Egle et al., 2015). Struvite precipitation is also often not possible in industrial wastewater because it has little to no nitrogen (Robles et al., 2020) Additionally, research on recovery of struvite from other waste streams has been limited to pilot studies and does not allow for separate capture of phosphorus and ammonia (Rahman et al., 2014; Song et al., 2011).

Chemical precipitation using calcium, aluminum, and iron coagulants have also shown to be an effective means of chemical phosphorus removal, however in a typical activated sludge treatment plant, these precipitates will be immobilized in the sludge as well (Sengupta et al., 2015). Some systems try to combat this by using chemical precipitation to treat the supernatant from sludge digesters, but the recovery potential is still low, around 30% (Egle et al., 2015). During direct anaerobic treatment of wastewater, nitrogen and phosphorus remain mobile as soluble ammonia and phosphate, which prevents their immobilization in the sludge and allows for exclusive capture of each of these nutrients in a subsequent downstream process, such as coagulation and flocculation.

Anaerobic membrane bioreactors (AnMBRs) represent an emerging environmental biotechnology platform with the potential to simultaneously recover water, energy, as well as nutrients from a variety of different concentrated wastewaters (Liao et al., 2006; Lin et al., 2013). AnMBRs combine the techniques of anaerobic biological treatment and membrane filtration, allowing for treatment of high strength wastewater to high effluent standards with a significantly reduced footprint (Lim et al., 2019). The AnMBR simultaneously produces methane from anaerobic processes along with a high-quality effluent containing nitrogen and phosphorus in the liquid phase that can either be captured separately or left in the water and applied as fertigation (Robles et al., 2020). Because of the high organic strength of swine waste, it is a prime candidate for AnMBR treatment and resource recovery, but there are limited studies on treatment of swine manure and swine wastewater by AnMBRs (Bu et al., 2017; D. Cheng et al., 2021). Additionally, AnMBRs present another challenge for providing high quality effluent: the presence of sulfate-reducing bacteria (SRBs), which reduce the sulfate from the influent to hydrogen sulfide (Damodara Kannan et al., 2020).

Sulfur in the form of sulfide also poses water quality issues, consuming the dissolved oxygen and creating negative impacts on the water's taste and odor (Kristiana et al., 2010). This odor comes in the form of hydrogen sulfide gas, a harmful gas with an Occupational Safety and Health Administration (OSHA) exposure limit at 20 ppm (U.S. Department of Labor, 2020). There is no published standard for treated effluent wastewater sulfide concentration, but the EPA has a criterion of 0.002 mg/L according to their 1986 water quality "gold book" (U.S. EPA, 2007). Sulfide and phosphate will both be present in municipal wastewater effluent after treatment through an anaerobic membrane bioreactor, requiring a tertiary treatment process for removal or recovery.

Iron phosphate recovery and calcium phosphate recovery are two chemical precipitation processes that have the potential to produce slow-release fertilizers to be used as alternatives to struvite. Although a market has emerged for struvite, detailed agronomic studies and techno-economic analyses on iron and calcium phosphate products are limited (Cornel & Schaum, 2009; Mayer et al., 2016; Robles et al., 2020).

1.1.1.1 Iron Phosphate Recovery

Iron addition via ferric chloride is a common practice for wastewater treatment plants to control odor from hydrogen sulfide formation, with dosing done at the headworks or upstream in the collection system to form iron sulfide (FeS) (Gutierrez et al., 2010). The mineral vivianite ($Fe_3(PO_4)_2*8H_2O$) is also known to precipitate out from municipal wastewater in anaerobic systems when residual ferrous iron is present, either from the wastewater itself or added during treatment, and is emerging as an alternative to struvite for phosphorus recovery (Rothe et al., 2016; Wilfert et al., 2018).There are unintended consequences to this process, however, with vivianite forming in sewer pipes and ferric chloride inhibiting methane production in anaerobic digesters (X. Cheng et al., 2017; Gutierrez et al., 2010; Wilfert et al., 2018).

Similar to struvite, vivianite is also considered to be a slow-release fertilizer (Robles et al., 2020; Y. Wu et al., 2019), but it does not have the same drawbacks of struvite, as stated previously: a relatively low P sequestration efficiency, the requirement of EBPR, and complex process controls (Ewert et al., 2014; Egle et al., 2015). Vivianite tends to precipitate out at neutral pH, which is typically the pH in wastewater streams, meaning it tends to happen naturally as long as iron is present (Y. Wu et al., 2019). Vivianite also has potential applications in the electronics industry, as well as agriculture, in addition to having a relatively stable market value (Y. Wu et al., 2019). Some of the drawbacks of vivianite recovered from wastewater are that it tends to get trapped in

the sludge (Robles et al., 2020; Y. Wu et al., 2019), although magnetic separation has had some success (Wilfert, P.K. et al., n.d.), and that its plant uptake capacity has yet to be evaluated. Various iron hydroxide minerals, such as lepidocrocite and ferrihydrite, in addition to amorphous iron phosphate minerals are also known to precipitate out from wastewater dosed with iron (H. Wu et al., 2015).

Coagulation of phosphate in the presence of sulfide is a novel process, of which only a few published studies exist (Dong et al., 2015; Yang & Bae, 2014). The study from South Korea demonstrated that sulfide and phosphorus removals were consistently above 99% and 80%, respectively, when using a ferric chloride ($FeCl_3$) dose at a molar ratio of 2.0 Fe^{3+}/S^{2-}, significantly greater than the stoichiometric ratio of 0.67 Fe^{3+}/S^{2-} required for sulfide removal (Yang & Bae, 2014). However, this study did not focus on recovery and characterization of these nutrients (Yang & Bae, 2014). Concomitant removal of sulfide and phosphorus from anaerobic centrates necessitates a higher coagulant dose, apart from other challenges such as the impact of residual organic matter in the permeate on nutrient capture efficiency and settleability of the precipitated product.

The addition of ferric chloride releases Fe^{3+} ions, which reduce to Fe^{2+} ions as they oxidize sulfide to sulfur (Gutierrez et al., 2010; Haaning Nielsen et al., 2005; Yang & Bae, 2014).These newly formed Fe^{2+} ions then precipitate out as FeS (Gutierrez et al., 2010; Haaning Nielsen et al., 2005; Yang & Bae, 2014). The released Fe^{3+} ions will also precipitate out phosphorus as $FePO_4*2H_2O$ (Yang & Bae, 2014; Zhang et al., 2010).

1.1.1.2 Calcium Phosphate Recovery

Another target for chemical phosphorus precipitation processes in wastewater is calcium phosphates (Robles et al., 2020). Calcium phosphates are a strong candidate for recovery because

it is similar in structure to commercial phosphate fertilizers, as well as phosphate mineral rock, which also has a high calcium content, giving it a higher potential to be recovered for other applications, in addition to fertilizers for crop production (Law & Pagilla, 2018; Lei et al., 2017). However, the commercial calcium phosphate fertilizers, single superphosphate (SSP) and triple superphosphate (TSP) are produced not by precipitation, but by the reaction of sulfuric acid with phosphate minerals (Cordell & White, 2013). One drawback of calcium precipitation processes is that there are no studies showing a potential for sulfide removal, while iron preferentially removes sulfide.

The precipitation reactions for calcium phosphate, depending on speciation of phosphate due to pH, are shown below in Equations 1-5 (Tran et al., 2014).

$5Ca^{2+} + 3PO_4^{3-} + OH^- \longrightarrow Ca_5(PO_4)_3(OH)$ (Hydroxyapatite) (Eq 1)

$4Ca^{2+} + H^+ + 3PO_4^{3-} + 3H_2O \longrightarrow Ca_4H(PO_4)_3*3H_2O$ (Octa calcium phosphate) (Eq 2)

$3Ca^{2+} + 2PO_4^{3-} \longrightarrow Ca_3(PO_4)_2$ (Tricalcium phosphate) (Eq 3)

$Ca^{2+} + HPO_4^{2-} \longrightarrow CaHPO_4$ (Monotite) (Eq 4)

$Ca^{2+} + HPO_4^{2-} \longrightarrow CaHPO_4*2H_2O$ (Brushite) (Eq 5)

pH, temperature, supersaturation level, and Ca/P molar ratio all play a role in determining the mineral form of the amorphous or crystalline calcium phosphate (Tran et al., 2014). Brushite and Monotite form near or below neutral pH, while hydroxyapatite, octa calcium phosphate, and tricalcium phosphate form at higher pH, with most calcium phosphate precipitation occurring above a pH of 9 (Law & Pagilla, 2018; Tran et al., 2014). All of these products formed in Equations 1-5 are potential slow-release fertilizers (Robles et al., 2020). There have been some work on

recovering brushite, with one study leading to the development of the commercial CalPrex process (Law & Pagilla, 2018), but most research is focused on recovering hydroxyapatite (Lei et al., 2017; Robles et al., 2020; Tran et al., 2014; Zheng et al., 2020). Hydroxyapatite precipitation occurs at pH above 7 and requires a Ca/P ratio of 1.67, but it has been shown that higher pH and higher Ca/P ratio increases recovery efficiency (Tran et al., 2014). However, techno-economic analysis of hydroxyapatite precipitation has not been well studied (Law & Pagilla, 2018).

Research on precipitation of calcium phosphate has been conducted using various methods for providing calcium to the system including, calcium chloride addition (Tran et al., 2014), calcium oxide (lime) addition (Hasegawa et al., 2017; Zheng et al., 2020), and relying on residual calcium in the wastewater (Lei et al., 2017; Tervahauta et al., 2014). One advantage of using lime is in wastewaters near neutral pH, the hydroxide ions produced from its addition will produce more alkaline conditions, increasing phosphorus precipitation efficiency (Zheng et al., 2020).While several studies have used lime for phosphorus precipitation in municipal waste (Zheng et al., 2020), research on using lime to recover phosphorus in swine waste is limited (Hasegawa et al., 2017)**.**

1.1.2 Microbial Electrochemical Systems

Microbial electrochemical systems (MES) are another method being explored for nutrient recovery. The most common and heavily research MES are microbial fuel cells (MFCs). Most MFCs contain two electrodes, an anode and a cathode separated by an ion exchange membrane, typically a proton exchange membrane (PEM), although anion exchange membranes (AEM) are now being used as well and have shown to be more effective at proton transfer (Rahimnejad et al, 2015). Electoractive bacteria oxidize organic electron donors and use the anode surface as an electron acceptor, as the anode chamber is operated under anaerobic conditions, devoid of

competing acceptors (Parameswaran et al., 2009). Protons are transferred through the membrane and electrons flow through the external circuit (Noori et al., 2019) to the cathode, where there is sufficient supply of oxygen for them to react with to form water (M. Li et al., 2018). The electroactive bacteria most common on MFC biofilms have been identified to be from the *Shewanella*, *Geobacteraceae*, and *Pseudomonas* families (Parameswaran et al., 2009). Bacteria from the genus *Geobacter sulfurreducens* has been shown to be the dominant member of the microbial community in acetate-fed biofilms, which can be cultivated from diverse environmental inocula including anaerobic digested sludge (Parameswaran et al., 2011; Torres et al., 2009). MFCs can also be operated as microbial electrolysis cells (MECs), producing hydrogen instead of electrical power (Logan et al., 2006; Parameswaran et al., 2009). This can be achieved by applying a small positive potential between the anode and cathode, as well as providing anoxic media to the cathode instead of air or dissolved oxygen in water (Logan et al., 2006; Rahimnejad et al., 2015). The primary research driver of using MES for nutrient recovery is that it reduces chemical costs associated with crystallization processes while sustainably harnessing the chemical energy from the wastewater to drive the electrochemical precipitation processes. Microbial electrochemical systems can enhance local phosphate concentration, as well as cation concentrations, through migration and charge transport to effectively precipitate out phosphorus products solely using the ion gradients naturally present in the waste stream, or possibly a sacrificial electrode to provide the required cations (Ge et al., 2017; N. Li et al., 2020).

1.2 Thesis Structure/Overview

The focus of this thesis is to evaluate phosphorus removal systems downstream form an AnMBR. The following objectives will be evaluated:

Objective 1: Evaluate performance of coagulation-flocculation-sedimentation systems for the simultaneous removal of phosphorus and sulfide from wastewater permeate after treatment through an anaerobic membrane bioreactor (AnMBR).

Objective 2: Assess the efficiency of iron phosphate recovery form wastewater and its potential as a fertilizer.

Objective 3: Tailor chemical addition of calcium to form the most available calcium phosphate product.

Objective 4: Compare the Coulombic recovery from acetate-fed and glucose-fed microbial electrochemical systems to determine the feasibility of directly feeding wastewater for capacitive deionization of phosphate.

This thesis is organized into 4 chapters with references at the end of each of them. **Chapters 2 and 3** will each focus on an individual chemical-based coagulation-flocculation-sedimentation (CFS) system to remove phosphorus from AnMBR wastewater permeate, addressing **Objective 1. Chapter 2** will discuss the results from a study published in the *Science of the Total Environment* (Heronemus et al., 2021) on iron phosphate recovery from municipal wastewater in the presence of sulfide and the effects caused by COD, as well as address **Objective 2. Chapter 3** will discuss a calcium phosphate precipitation process to tailor the treatment of swine wastewater to recover a more efficient product, as described in **Objective 3. Chapter** 4 addresses **Objective 4** with preliminary experiments on microbial electrolysis cells necessary for future work on using a microbial electrochemical system along with electrocoagulation to recover nutrients by capacitive deionization.

1.3 References

Bashar, R., Gungor, K., Karthikeyan, K. G., & Barak, P. (2018). Cost effectiveness of phosphorus removal processes in municipal wastewater treatment. *Chemosphere (Oxford)*, *197*, 280–290. https://doi.org/10.1016/j.chemosphere.2017.12.169

Bu, F., Du, S., Xie, L., Cao, R., & Zhou, Q. (2017). Swine manure treatment by anaerobic membrane bioreactor with carbon, nitrogen and phosphorus recovery. *Water Science and Technology*, *76*(7–8), 1939–1949. https://doi.org/10.2166/wst.2017.278

Cheng, D., Ngo, H. H., Guo, W., Chang, S. W., Nguyen, D. D., Nguyen, Q. A., Zhang, J., & Liang, S. (2021). Improving sulfonamide antibiotics removal from swine wastewater by supplying a new pomelo peel derived biochar in an anaerobic membrane bioreactor. *Bioresource Technology*, *319*, 124160–124160. https://doi.org/10.1016/j.biortech.2020.124160

Cheng, H.-H., Narindri, B., Chu, H., & Whang, L.-M. (2020). Recent advancement on biological technologies and strategies for resource recovery from swine wastewater. *Bioresource Technology*, *303*, 122861–122861. https://doi.org/10.1016/j.biortech.2020.122861

Cheng, X., Wang, J., Chen, B., Wang, Y., Liu, J., & Liu, L. (2017). Effectiveness of phosphate removal during anaerobic digestion of waste activated sludge by dosing iron(III). *Journal of Environmental Management*, *193*, 32–39. https://doi.org/10.1016/j.jenvman.2017.02.009

Cordell, D., Rosemarin, A., Schröder, J. J., & Smit, A. L. (2011). Towards global phosphorus security: A systems framework for phosphorus recovery and reuse options. *Chemosphere (Oxford)*, *84*(6), 747–758. https://doi.org/10.1016/j.chemosphere.2011.02.032

Cordell, Dana, Drangert, J.-O., & White, S. (2009). The story of phosphorus: Global food security and food for thought. *Global Environmental Change*, *19*(2), 292–305. https://doi.org/10.1016/j.gloenvcha.2008.10.009

Cordell, Dana, & White, S. (2013). Sustainable Phosphorus Measures: Strategies and Technologies for Achieving Phosphorus Security. *Agronomy (Basel)*, *3*(1), 86–116. https://doi.org/10.3390/agronomy3010086

Cornel, P., & Schaum, C. (2009). Phosphorus recovery from wastewater: Needs, technologies and costs. *Water Science and Technology*, *59*(6), 1069–1076. https://doi.org/10.2166/wst.2009.045

Damodara Kannan, A., Evans, P., & Parameswaran, P. (2020). Long-term microbial community dynamics in a pilot-scale gas sparged anaerobic membrane bioreactor treating municipal wastewater under seasonal variations. *Bioresource Technology*, *310*, 123425–123425. https://doi.org/10.1016/j.biortech.2020.123425

David W Schindler, R E Hecky, D L Findlay, M P Stainton, B R Parker, M J Paterson, K G Beaty, M Lyng, & S E M Kasian. (2008). Eutrophication of Lakes Cannot Be Controlled by Reducing Nitrogen Input: Results of a 37-Year Whole-Ecosystem Experiment. *Proceedings of*

the National Academy of Sciences - PNAS, *105*(32), 11254–11258. https://doi.org/10.1073/pnas.0805108105

Dodds, W. K., Bouska, W. W., Eitzmann, J. L., Pilger, T. J., Pitts, K. L., Riley, A. J., Schloesser, J. T., & Thornbrugh, D. J. (2009). Eutrophication of U.S. Freshwaters: Analysis of Potential Economic Damages. *Environmental Science & Technology*, *43*(1), 12–19. https://doi.org/10.1021/es801217q

Dong, Q., Parker, W., & Dagnew, M. (2015). Impact of FeCl3 dosing on AnMBR treatment of municipal wastewater. *Water Research (Oxford)*, *80*, 281–293. https://doi.org/10.1016/j.watres.2015.04.025

Egle, L., Rechberger, H., & Zessner, M. (2015). Overview and description of technologies for recovering phosphorus from municipal wastewater. *Resources, Conservation and Recycling*, *105*, 325–346. https://doi.org/10.1016/j.resconrec.2015.09.016

Ewert, W., Hermanussen, O., Kabbe, C., Mele, C., Niewersch, H., Paillard, H., St€ossel, E., Wagenbach, A., Steman, J. (2014). Sustainable Sewage Sludge Management Fostering Phosphorus Recovery and Energy Efficiency.

Ge, Z., Chen, X., & Ren, Z. (2017). Capacitive Deionization for Nutrient Recovery from Wastewater with Disinfection Capability. *Environ. Sci.: Water Res. Technol.*, *4*. https://doi.org/10.1039/C7EW00350A

Gutierrez, O., Park, D., Sharma, K. R., & Yuan, Z. (2010). Iron salts dosage for sulfide control in sewers induces chemical phosphorus removal during wastewater treatment. *Water Research (Oxford)*, *44*(11), 3467–3475. https://doi.org/10.1016/j.watres.2010.03.023

Haaning Nielsen, A., Lens, P., Vollertsen, J., & Hvitved-Jacobsen, T. (2005). Sulfide–iron interactions in domestic wastewater from a gravity sewer. *Water Research (Oxford)*, *39*(12), 2747–2755. https://doi.org/10.1016/j.watres.2005.04.048

Hasegawa, T., Kurose, Y., & Tanaka, Y. (2017). Advanced treatment technique for swine wastewater using two agents: Thermally polymerized amorphous silica and hydrated lime for color and phosphorus removal and sulfur for nitrogen removal. *Animal Science Journal*, *88*(10), 1636–1643. https://doi.org/10.1111/asj.12803

Henze, M., van Loosdrecht, M. C. M., Ekama, G. A., & Brdjanovic, D. (2008). *Biological Wastewater Treatment: Principles, Modelling and Design*. IWA Publishing.

Heronemus, E., Gamage, K. H. H., Hettiarachchi, G. M., & Parameswaran, P. (2021). Efficient recovery of phosphorus and sulfur from Anaerobic Membrane Bioreactor (AnMBR) permeate using chemical addition of iron and evaluation of its nutrient availability for plant uptake. *Science of The Total Environment*, *783*, 146850. https://doi.org/10.1016/j.scitotenv.2021.146850

Kristiana, I., Heitz, A., Joll, C., & Sathasivan, A. (2010). Analysis of polysulfides in drinking water distribution systems using headspace solid-phase microextraction and gas

chromatography–mass spectrometry. *Journal of Chromatography A*, *1217*(38), 5995–6001. https://doi.org/10.1016/j.chroma.2010.07.051

Law, K. P., & Pagilla, K. R. (2018). Phosphorus Recovery by Methods Beyond Struvite Precipitation. *Water Environment Research*, *90*(9), 840–850. https://doi.org/10.2175/106143017X15131012188006

Lei, Y., Song, B., van der Weijden, R. D., Saakes, M., & Buisman, C. J. N. (2017). Electrochemical Induced Calcium Phosphate Precipitation: Importance of Local pH. *Environmental Science & Technology*, *51*(19), 11156–11164. https://doi.org/10.1021/acs.est.7b03909

Li, M., Zhou, M., Tian, X., Tan, C., McDaniel, C. T., Hassett, D. J., & Gu, T. (2018). Microbial fuel cell (MFC) power performance improvement through enhanced microbial electrogenicity. In *Biotechnology Advances* (Vol. 36, Issue 4, pp. 1316–1327). Elsevier Inc. https://doi.org/10.1016/j.biotechadv.2018.04.010

Li, N., Wan, Y., & Wang, X. (2020). Nutrient conversion and recovery from wastewater using electroactive bacteria. *Science of The Total Environment*, *706*, 135690. https://doi.org/10.1016/j.scitotenv.2019.135690

Liao, B.-Q., Kraemer, J. T., & Bagley, D. M. (2006). Anaerobic Membrane Bioreactors: Applications and Research Directions. *Critical Reviews in Environmental Science and Technology*, *36*(6), 489–530. https://doi.org/10.1080/10643380600678146

Lim, K., Evans, P. J., & Parameswaran, P. (2019). Long-Term Performance of a Pilot-Scale Gas-Sparged Anaerobic Membrane Bioreactor under Ambient Temperatures for Holistic Wastewater Treatment. *Environmental Science & Technology*, *53*(13), 7347–7354. https://doi.org/10.1021/acs.est.8b06198

Lin, H., Peng, W., Zhang, M., Chen, J., Hong, H., & Zhang, Y. (2013). A review on anaerobic membrane bioreactors: Applications, membrane fouling and future perspectives. *Desalination*, *314*, 169–188. https://doi.org/10.1016/j.desal.2013.01.019

Logan, B. E., Hamelers, B., Rozendal, R., Schröder, U., Keller, J., Freguia, S., Aelterman, P., Verstraete, W., & Rabaey, K. (2006). Microbial Fuel Cells: Methodology and Technology. *Environmental Science & Technology*, *40*(17), 5181–5192. https://doi.org/10.1021/es0605016

Mayer, B. K., Baker, L. A., Boyer, T. H., Drechsel, P., Gifford, M., Hanjra, M. A., Parameswaran, P., Stoltzfus, J., Westerhoff, P., & Rittmann, B. E. (2016). Total Value of Phosphorus Recovery. *Environmental Science & Technology*, *50*(13), 6606–6620. https://doi.org/10.1021/acs.est.6b01239

Meinen, R. J., Kephart, K. B., & Graves, R. E. (2014). Economic feasibility and evaluation of a novel manure collection and anaerobic digestion system at a commercial swine finisher enterprise. *Biomass and Bioenergy*, *63*, 10–21. https://doi.org/10.1016/j.biombioe.2014.01.032

Nelson, N. O., Mikkelsen, R. L., & Hesterberg, D. L. (2003). Struvite precipitation in anaerobic swine lagoon liquid: Effect of pH and Mg:P ratio and determination of rate constant. *Bioresource Technology*, *89*(3), 229–236. https://doi.org/10.1016/S0960-8524(03)00076-2

Noori, M. T., Ghangrekar, M. M., Mukherjee, C. K., & Min, B. (2019). Biofouling effects on the performance of microbial fuel cells and recent advances in biotechnological and chemical strategies for mitigation. In *Biotechnology Advances* (Vol. 37, Issue 8, p. 107420). Elsevier Inc. https://doi.org/10.1016/j.biotechadv.2019.107420

Otoo, M., Drechsel, P., & Hanjra, M. A. (2015). *Business Models and Economic Approaches for Nutrient Recovery from Wastewater and Fecal Sludge* (pp. 247–268). Springer Netherlands. https://doi.org/10.1007/978-94-017-9545-6_13

Parameswaran, P., Torres, C. I., Lee, H.-S., Krajmalnik-Brown, R., & Rittmann, B. E. (2009). Syntrophic interactions among anode respiring bacteria (ARB) and Non-ARB in a biofilm anode: Electron balances. *Biotechnology and Bioengineering*, *103*(3), 513–523. https://doi.org/10.1002/bit.22267

Parameswaran, P., Torres, C. I., Lee, H.-S., Rittmann, B. E., & Krajmalnik-Brown, R. (2011). Hydrogen consumption in microbial electrochemical systems (MXCs): The role of homo-acetogenic bacteria. *Bioresource Technology*, *102*(1), 263–271. https://doi.org/10.1016/j.biortech.2010.03.133

Pastor, L., Mangin, D., Ferrer, J., & Seco, A. (2010). Struvite formation from the supernatants of an anaerobic digestion pilot plant. *Bioresource Technology*, *101*(1), 118–125. https://doi.org/10.1016/j.biortech.2009.08.002

Rahimnejad, M., Adhami, A., Darvari, S., Zirepour, A., & Oh, S.-E. (2015). Microbial fuel cell as new technology for bioelectricity generation: A review. *Alexandria Engineering Journal*, *54*(3), 745–756. https://doi.org/10.1016/j.aej.2015.03.031

Rahman, M. M., Salleh, M. A. M., Rashid, U., Ahsan, A., Hossain, M. M., & Ra, C. S. (2014). Production of slow release crystal fertilizer from wastewaters through struvite crystallization – A review. *Arabian Journal of Chemistry*, *7*(1), 139–155. https://doi.org/10.1016/j.arabjc.2013.10.007

Robert J Diaz & Rutger Rosenberg. (2008). Spreading Dead Zones and Consequences for Marine Ecosystems. *Science (American Association for the Advancement of Science)*, *321*(5891), 926–929. https://doi.org/10.1126/science.1156401

Robles, Á., Aguado, D., Barat, R., Borrás, L., Bouzas, A., Giménez, J. B., Martí, N., Ribes, J., Ruano, M. V., Serralta, J., Ferrer, J., & Seco, A. (2020). New frontiers from removal to recycling of nitrogen and phosphorus from wastewater in the Circular Economy. *Bioresource Technology*, *300*, 122673–122673. https://doi.org/10.1016/j.biortech.2019.122673

Rothe, M., Kleeberg, A., & Hupfer, M. (2016). The occurrence, identification and environmental relevance of vivianite in waterlogged soils and aquatic sediments. *Earth-Science Reviews*, *158*, 51–64. https://doi.org/10.1016/j.earscirev.2016.04.008

Roychand, R., Kumar Pramanik, B., Zhang, G., & Setunge, S. (2020). Recycling steel slag from municipal wastewater treatment plants into concrete applications – A step towards circular economy. *Resources, Conservation and Recycling*, *152*, 104533-. https://doi.org/10.1016/j.resconrec.2019.104533

Sengupta, S., Nawaz, T., & Beaudry, J. (2015). Nitrogen and Phosphorus Recovery from Wastewater. *Current Pollution Reports*, *1*(3), 155–166. https://doi.org/10.1007/s40726-015-0013-1

Song, Y.-H., Qiu, G.-L., Yuan, P., Cui, X.-Y., Peng, J.-F., Zeng, P., Duan, L., Xiang, L.-C., & Qian, F. (2011). Nutrients removal and recovery from anaerobically digested swine wastewater by struvite crystallization without chemical additions. *Journal of Hazardous Materials*, *190*(1), 140–149. https://doi.org/10.1016/j.jhazmat.2011.03.015

Tervahauta, T., van der Weijden, R. D., Flemming, R. L., Hernández Leal, L., Zeeman, G., & Buisman, C. J. (2014). Calcium phosphate granulation in anaerobic treatment of black water: A new approach to phosphorus recovery. *Water Research (Oxford)*, *48*(1), 632–642. https://doi.org/10.1016/j.watres.2013.10.012

Torres, C. I., Krajmalnik-Brown, R., Parameswaran, P., Marcus, A. K., Wanger, G., Gorby, Y. A., & Rittmann, B. E. (2009). Selecting Anode-Respiring Bacteria Based on Anode Potential: Phylogenetic, Electrochemical, and Microscopic Characterization. *Environmental Science & Technology*, *43*(24), 9519–9524. https://doi.org/10.1021/es902165y

Tran, A. T. K., Zhang, Y., De Corte, D., Hannes, J.-B., Ye, W., Mondal, P., Jullok, N., Meesschaert, B., Pinoy, L., & Van der Bruggen, B. (2014). P-recovery as calcium phosphate from wastewater using an integrated selectrodialysis/crystallization process. *Journal of Cleaner Production*, *77*, 140–151. https://doi.org/10.1016/j.jclepro.2014.01.069

U.S. Department of Labor, Hydrogen Sulfide. https://www.osha.gov/hydrogen-sulfide. Accessed 22 February 2020.

U.S. EPA. (2007). Quality Criteria for Water 1986 (Report No. 440/5-86-001). 1-395.

Wilfert, P., Dugulan, A. I., Goubitz, K., Korving, L., Witkamp, G. J., & Van Loosdrecht, M. C. M. (2018). Vivianite as the main phosphate mineral in digested sewage sludge and its role for phosphate recovery. *Water Research (Oxford)*, *144*, 312–321. https://doi.org/10.1016/j.watres.2018.07.020

Wilfert, P.K., van Loosdrecht, Mark C.M., Witkamp, G.J., & Delft University of Technology. (n.d.). *Phosphate Recovery From Sewage Sludge Containing Iron Phosphate*. https://doi.org/10.4233/uuid:f3729790-0cfe-4f92-866b-eca3f2f2df24

Wu, H., Ikeda-Ohno, A., Wang, Y., & Waite, T. D. (2015). Iron and phosphorus speciation in Fe-conditioned membrane bioreactor activated sludge. *Water Research (Oxford)*, *76*, 213–226. https://doi.org/10.1016/j.watres.2015.02.020

Wu, Y., Luo, J., Zhang, Q., Aleem, M., Fang, F., Xue, Z., & Cao, J. (2019). Potentials and challenges of phosphorus recovery as vivianite from wastewater: A review. *Chemosphere (Oxford)*, *226*, 246–258. https://doi.org/10.1016/j.chemosphere.2019.03.138

Yang, S., & Bae, J. (2014). A feasibility of coagulation as post-treatment of the anaerobic fluidized bed reactor (AFBR) treating domestic wastewater. *Journal of the Korean Society of Water and Wastewater*, *28*(6), 623–634. https://doi.org/10.11001/jksww.2014.28.6.623

Zhang, T., Ding, L., Ren, H., Guo, Z., & Tan, J. (2010). Thermodynamic modeling of ferric phosphate precipitation for phosphorus removal and recovery from wastewater. *Journal of Hazardous Materials*, *176*(1), 444–450. https://doi.org/10.1016/j.jhazmat.2009.11.049

Zheng, X., Ye, Y., Jiang, Z., Ying, Z., Ji, S., Chen, W., Wang, B., & Dou, B. (2020). Enhanced transformation of phosphorus (P) in sewage sludge to hydroxyapatite via hydrothermal carbonization and calcium-based additive. *Science of The Total Environment*, *738*, 139786. https://doi.org/10.1016/j.scitotenv.2020.139786

Chapter 2 - Phosphorus Precipitation by Iron Addition

2.1 Introduction

Recovered nutrient products (RNPs) may differ in nutrient composition depending on the wastewater composition, wastewater characteristics and the treatment technologies applied. These recovered phosphorus rich nutrient products may contain high concentrations of other metals and anionic ligands, in addition to iron and phosphate, affecting phosphorus release and availability to plants. Although phosphorus in these iron-based RNPs could be a suitable phosphorus fertilizer source for some soils, their physical and chemical heterogeneous nature could lead to varying characteristics and behavior in soils. Characterization of these RNPs is important to understand the potential availability of nutrients when it is applied as a soil amendment or fertilizer.

The key objective of this chapter is to assess the efficiency of iron phosphate recovery form wastewater and its potential as a fertilizer. This was accomplished through four secondary objectives: to optimize the coagulant doses through batch jar tests of synthetic AnMBR permeate to achieve simultaneous removal of phosphorus and sulfide at varying chemical oxygen demand (COD) concentrations, to adjust the coagulant dosage for actual AnMBR permeate through additional batch jar tests, to evaluate whether the phosphorus and sulfide recovery goals can be achieved consistently during continuous operation of the pilot scale AnMBR's CFS unit, and to characterize the solid recovered nutrient products and evaluate its transformations in soil, through detailed soil studies for its phosphorus release rate and potential availability for plant uptake.

2.2 Materials and Methods

2.2.1 Bench Scale Jar Testing

Manhattan Wastewater Treatment Plant's secondary clarifier effluent was collected to be used as the model permeate. Sulfide, ammonium, and total phosphorus were added to the effluent to reach

the desired levels that mimicked the AnMBR permeate from the pilot scale demonstration: 5 mg/L P, 40 mg/L NH_4-N, and 28.2 mg/L sulfide-S^{2-}. Next, the COD was adjusted to the appropriate concentration, with three levels tested: 22.8 mg/L, 45 mg/L, and 200 mg/L. The lowest COD concentration (22.8 mg/L) represents the average COD from the Manhattan wastewater clarifier effluent. To achieve the 45 mg/L and 200 mg/L concentrations of COD, volatile fatty acids (VFAs) were used to increase the COD of the synthetic permeate. Based on actual distribution of VFAs in the pilot scale AnMBR permeate from Ft. Riley, as quantified by high performance liquid chromatograph (HPLC) analysis (Shimadzu Scientific, USA), acetic acid and isovaleric acid were added to increase the COD level to 45 mg/L, and a combination of acetic acid, isobutyric acid, isovaleric acid, and valeric acid was added to increase the COD to 200 mg/L (Evans et al., 2018). The HPLC (Shimadzu LC-20AT, USA) uses an Aminex HPX-87H column (Bio-Rad Laboratories, USA) to separate the organic acids and alcohols which then were detected by a photo diode array and refractive index detectors (Lim et al., 2019). It should be noted that the sulfide addition was made after the COD was dosed to the appropriate levels based on VFA data, so the sulfide COD is not factored in. Once the synthetic permeate was appropriately dosed, initial conditions of dissolved iron, total phosphorus, sulfide, and pH were recorded. The pH of the synthetic permeates ranged from 7-8 based on the condition of the collected wastewater effluent.

Stock solutions of aluminum chlorohydrate (ACH) and $FeCl_3$ were prepared to reach densities of 0.267 g/mL and 1.411 g/mL respectively. The coagulants were then added from these stock solutions to four beakers filled with 1 L of the synthetic permeate. Each set of jar tests was divided into two sets, corresponding to four doses of the coagulant aid (ACH), ranging from 16.9 to 67.5 mg/L Al, for each of the two $FeCl_3$ doses, 121.5 and 182.2 mg/L Fe. This dosing matrix is shown explicitly in **Table 2.1**. The beakers were then rapidly mixed at 100 RPM for two minutes, after

which the mixing speed was reduced to 30 RPM for 20 minutes. The jars were mixed using a Phipps & Bird Stirrer (model 7790-400). Once the slow mixing was completed, the contents of each jar were placed in 1000 mL graduated cylinders to settle for 30 minutes to evaluate sludge settleability. Once settleability was assessed, a sample was collected from the top two inches of the graduated cylinder and tested for turbidity. A liquid sample was collected from each cylinder and filtered through a 1.2 μm GF/C filter. The filtered samples were then tested for residual sulfide, total phosphorus, and dissolved iron. The unfiltered waste in each cylinder was finally tested for pH.

Table 2.1. Coagulant dosing for various combinations of ACH at each $FeCl_3$ dose, giving 8 different conditions to test for each COD level for experiments with synthetic permeate.

Set 1				Set 2			
ACH Concentration		**$FeCl_3$ Concentration**		**ACH Concentration**		**$FeCl_3$ Concentration**	
(mg/L as Al)	(mM)	(mg/L as Fe)	(mM)	(mg/L as Al)	(mM)	(mg/L as Fe)	(mM)
16.9	0.63	121.5	2.17	16.9	0.63	182.2	3.26
33.7	1.25			33.7	1.25		
50.6	1.88			50.6	1.88		
67.5	2.50			67.5	2.50		

2.2.2 Bench Scale Analytical Methods

Initial and residual dissolved sulfide tests were conducted using the USEPA Methylene Blue Method (Method 8131). Dissolved iron tests were conducted using USEPA FerroVer Method (Method 8008). A HACH DR 1900 spectrophotometer was used for dissolved sulfide and iron analyses. For the jar tests at 22.8 mg/L COD, total phosphorus was measured before and after coagulation using an inductively coupled plasma optical emission spectrometer or ICP-OES (720-ES, Varian, Santa Clara, CA). However, for the remaining tests, HACH TNT 843 kits (concentration range 0.05 – 1.5 mg/L as P) were used to measure total phosphorus. Previous testing in this lab has shown these two methods to give results within 15% of each other. COD

concentrations were verified using HACH TNT 820, 821, and 822 kits (concentration range 1-60 mg/L, 3-150 mg/L, and 20-1500 mg/L, respectively). The HACH kits were analyzed using the HACH DR 3900 spectrophotometer. Turbidity analysis was conducted using a HACH 2100Q portable turbidimeter. pH analysis was conducted using a VWR sympHony B10P pH benchtop meter.

2.2.3 Ft. Riley Testing and Pilot Plant Operation

Jar testing was conducted in the pilot scale AnMBR site using the same method as described in the section 2.1, with the exceptions that actual permeate from the AnMBR was used rather than using a synthetic recipe and a cationic polymer was additionally added to aid settleability at a concentration of 1 mg/L. The polymer addition was to ensure adequate settleability for a wastewater derived product. Liquid grab samples were used to measure the phosphorus and sulfide levels at different stages of the treatment process (Lim et al., 2019). Residual sulfide was measured using similar methods employed for the bench scale jar test analysis, while total phosphorus was measured using an OI Analytical Alpkem RFA300 rapid flow analyzer (Lim et al., 2019). Ferric chloride and ACH concentrations of 110 mg/L as Fe, 30 mg/L as Al, and a cationic polymer at 1 mg/L were used for the continuous pilot scale CFS unit (Lim et al., 2019).

2.2.4 Characterization and Plant Uptake Potential of Recovered Nutrient Product

2.2.4.1 Product Characterization

The original RNP sample, collected from the pilot scale AnMBR CFS unit during steady state operation, was freeze-dried and digested using USEPA method SW846-3051A (USEPA, 2007). The digestate was analyzed for the nutrient composition as well as for selected potentially toxic trace elements using an ICP-OES and an inductively coupled plasma mass spectrometer or ICP-MS (7500cx, Agilent, Santa Clara, CA). A powder XRD analysis was conducted to identify

existing nutrient phases in the RNP using PANalytical Empyrean Multi-Purpose X-Ray Diffractometer (Spectris Company, Egham, Surrey, UK) with a copper anode material and generator settings of 35 eV and 20 mA. Due to expected amorphous nature of the products, scanning electron microscope (SEM) and energy dispersive spectroscopy analysis was also performed using a Hitachi S-3500N scanning electron microscope equipped with a Model S-6542 absorbed electron detector (Hitachi Science Systems, Ibaraki, Japan) at an accelerating potential of 5 kV. X-ray absorption near-edge structure (XANES) spectroscopy analysis was conducted to further characterize the product at Sector 9-BM-B, Advanced Photon Source, Argonne National Laboratory, Argonne, IL. The RNP sample was diluted ten times using boron nitride. The sample was pelleted with a KBr Quick Press Kit (International Crystal Laboratories, Garfield, NJ) and carefully placed on a double-sided carbon tape (SPI Supplies, West Chester, PA) and placed on the sample holder. Six XANES scans were collected for the sample in fluorescence mode. Edge energy was calibrated using phosphorus pentoxide (P_2O_5). Background correction followed by the linear combination fitting of the reported spectra were done using previously collected standards in Athena (Ravel & Newville, 2005) according to the concepts of Werner & Prietzel (2015).

2.2.4.2 Potentially Plant Available Phosphorus Determination

A 5-week long laboratory incubation study was conducted using an alkaline, mildly calcareous silt loam soil from Garden City, Kansas. Iron phosphate has limited solubility therefore, we chose this soil for our experiments. Soil was collected at the depth of 10 cm, air-dried and sieved to < 2 mm. The pH of the soil was measured in a 1:10 soil: water extract (Watson and Brown, 1998) and available phosphorus (P) was measured by extraction with sodium bicarbonate (Olsen, 1954). The Cation Exchange Capacity (CEC) was determined by the displacement method (Soil Survey Staff, 2011); carbonates were determined according to Allison and Moodie (1965) and total P was

determined according to Zarcinas et al. (1996), which is then modified to use a digestion block instead of a microwave. The Maximum Water Holding Capacity (MWHC) was measured using the protocol from Jenkinson & Powlson (1976). Total organic C was determined via the dry combustion method of Nelson and Sommers (1996). Soil texture was determined using a combination of a modification of the pipette method by Kilmer & Alexander (1949) and Method 3A-1 from the Soil Survey Laboratory's methods manual (Soil Survey Laboratory Staff, 2004). Petri dishes (87 mm diameter and 11 mm height) were packed to a bulk density of 1.0 g cm^{-3} with 10% of the total deionized water needed for 55% soil's maximum water-holding capacity. Then by adding remaining deionized water slowly on to the packed soil, 55% maximum water-holding capacity was achieved. The plates were wrapped with Parafilm (Bemis Flexible Packaging, Neenah, WI), and left to equilibrate for 24 hours at room temperature. The plates were unwrapped, and the powdered treatments were placed in the center of the plate, just below the soil surface and covering with soil. There were four treatments with four replicates as follows:

i. Unfertilized control soil sample;
ii. Mono ammonium phosphate (MAP, 11:23:0; 11% N–23% P–0% K_2O by weight): 7.5 mg P;
iii. Triple superphosphate (TSP, 0:20:0; 0% N–20% P–0% K_2O by weight): 7.5 mg P); and
iv. RNP (2.6% P by weight): 7.5mg of P.

All fertilizer treatments received 7.5 mg P per petri plate. Petri dishes were closed and wrapped again with Parafilm (Bemis Flexible Packaging, Neenah, WI). Dishes were wrapped in aluminum foil and incubated (Precision Low Temp Incubator, Waltham, MA) in the dark at 25°C. This 5 weeks' time indicates critical P uptake for cereal crops (Hettiarachchi, 2010; Pierzynski & Hettiarachchi, 2018; Williams, 1948).

Plates were opened at the end of 5 weeks and the soil was collected from 0 to 7.5, 7.5 to 13.5, 13.5 to 25, and 25 to 43.5 mm, from the point of application as concentric rings. Each sample was placed in a pre-weighed plastic specimen container (Fisher Scientific, Waltham, MA). The samples were oven dried quickly at 40°C (Fisher Scientific drying oven, Waltham, MA). After drying, weight was recorded, and soils were ground gently with a mortar and pestle.

Total P for all samples was determined by aqua regia digestion (without H_2O_2 pretreatment) and analyzed via ICP-OES. Potentially plant available P was determined by the anion exchange resin (AER) technique (Myers et al., 2005) and quantified colorimetrically using a Beckman-Coulter DU-800 spectrophotometer (Brea, CA) (Murphy & Riley, 1962).

Percentage of resin P (PRP) for each dish section for all treatments were calculated according to the following equation (Pierzynski & Hettiarachchi, 2018):

$$PRP = \frac{PEP_i}{Total\ P_i} \times 100$$

where *i* is the dish section (1–4), REPi is the resin P concentration, and Total Pi is the total P concentration in the *i* dish section.

PROC MIXED procedure in SAS (SAS Institute, 2011) were used to analyze the soil data. The experimental design was a complete randomized design. Least Significance difference method was used to compare all treatments at a 0.05 level of significance.

2.3 Results and Discussion

2.3.1 Bench Scale Analysis with synthetic permeate

Bench scale testing was conducted to investigate changes in phosphorus and sulfide removal efficiencies as the coagulant doses and permeate COD concentrations were changed. The coagulant dosing matrix of $FeCl_3$ and ACH was developed by trial and error and evaluated based

on a project goal to achieve 90% removal of total phosphorus from the municipal wastewater influent of the AnMBR (Evans et al., 2018).

2.3.1.1 Phosphorus Removal - Coagulant Dosing Effects

Previous studies have shown that adding iron salts for chemical phosphorus precipitation in traditional wastewater treatment plants and aerobic membrane bioreactors can achieve P removals greater than 90% (Caravelli et al., 2010; Wang et al., 2014). At a permeate COD of 22.8 mg/L, phosphorus removal was consistently greater than 96% for each ferric chloride dose, as shown in **Figure 2.1a**. An increase in coagulant dose generally increased the phosphorus removal from less than 90% to 99%. Increasing the ferric chloride dose from 121.5 mg/L to 182.2 mg/L as Fe was shown to significantly increase the phosphorus removal for the synthetic permeate for COD values of 45 mg/L ($p = 0.005$) and 200 mg/L ($p = 0.006$). At this higher coagulant dose, the phosphorus removal percentage was always greater than 90%. The relationship between ferric chloride dose and phosphorus removal can be seen in **Figures 2.1 a-c**.

The impact of the coagulant aid, ACH, on settleability will be discussed in section 2.2.1.4**,** but ACH is also known to be capable of achieving some phosphorus removal as a primary coagulant (Hatton & Simpson, 1985). As illustrated in **Figure 2.1**, increasing the dose of ACH from 16.9 mg/L as Al to 33.7, 50.6, and 66.5 mg/L generally increased the phosphorus removal at each respective level, with an increase of over 20% seen at the highest COD level. This effect was more pronounced at the lower ferric chloride doses, where phosphorus removal efficiency was lower.

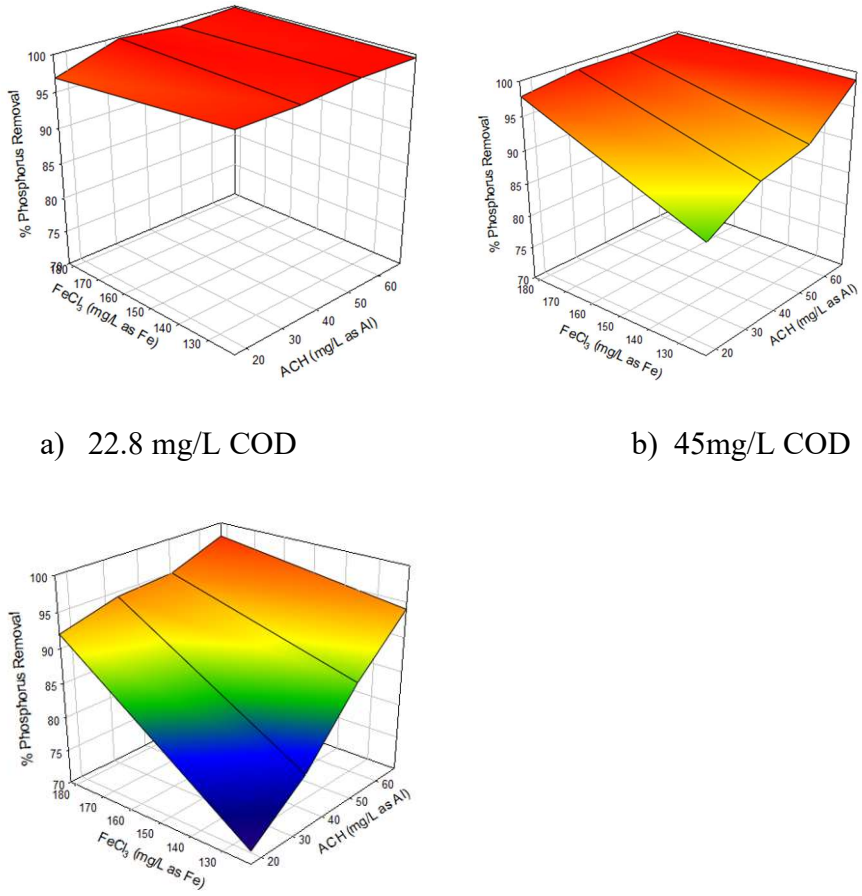

a) 22.8 mg/L COD

b) 45mg/L COD

c) 200mg/L COD

Figure 2.1 Phosphorus removal efficiency as a function of coagulants FeCl3 and ACH doses for jar tests at different COD levels. For increasing COD levels, Phosphorus removal efficiency dropped at the lower FeCl3 (less than 150 mg/L as Fe) and ACH (less than 40 mg/L) doses.

2.3.1.2 Phosphorus Removal - COD Effects

The bench scale study also shows a general decrease in phosphorus removal efficiencies as synthetic permeate COD increases, as can be seen by comparing **Figure 2.1 a, b,** and **c**. A significant decrease in phosphorus removal is seen when increasing the COD from 45 mg/L to 200 mg/L at the 121.5 mg/L ferric chloride dose ($p = 0.046$) and the 182.2 mg/L as Fe ferric chloride dose ($p=0.001$). It is likely that this was caused by complexing of the organics with phosphate in aqueous form. There are conflicting studies on the impact of organics on settleability and

phosphorus removal in coagulation (Inskeep & Silvertooth, 1988; Omoike & vanLoon, 1999; Zhou et al., 2008). Findings by Omoike & Vanloon (1999), as well as Inskeep & Silvertooth (1988) indicate that tannic acid can inhibit the precipitation of phosphorus. However, the study conducted by Zhou et al (2008) has shown that tannic acid can behave as a coagulant aid in phosphorus removal to ferric chloride. A higher COD created a greater demand for the addition of coagulant to reach comparable P removal efficiencies to that of the lower COD samples. However, a phosphorus removal efficiency above the 90% threshold was still met when the highest concentrations of $FeCl_3$ and ACH were applied, with phosphorus concentrations consistently below 1.5 mg/L P.

2.3.1.3 Sulfide Removal - Coagulant Dosing Effects and Impact of COD

Modeling in a previous study showed 98% removal of dissolved sulfide at a concentration of 7.6 mg/L from municipal wastewater with a dose of 30 mg/L $FeCl_3$ (Gutierrez et al., 2010). The jar testing setup, as described in Materials and Methods, consistently achieved a sulfide removal of 99.5% removal or greater for each ferric chloride and ACH combination. A 0.1 mg/L dissolved sulfide residual as S was chosen as a removal goal based on the capability of the AnMBR's CFS process (Lim et al., 2019). The two ferric chloride doses tested in this study, 121.5 mg/L Fe and 182.2 mg/L Fe, were well in excess of the previously mentioned stoichiometric ratio of 0.67 Fe^{3+}/S^{2-} at 2.5 and 3.7, respectively (Yang & Bae, 2014). Sulfide was consistently removed to concentrations below this goal at the higher ferric chloride dose, but the goal was not always met at the lower coagulant concentration. Although the residual reached after the coagulation process is significantly higher than the EPA criterion, it is likely to be further reduced downstream through sorption to clinoptilolite (a naturally occurring clay for ammonia adsorption from permeate) in the pilot scale AnMBR process train and some further losses by exposure to oxygen (Lim et al., 2019).

It should also be noted that increasing the ferric chloride dose did not always lead to increases in sulfide removal efficiency. This can be seen in **Figure 2.2** when examining the sulfide residual for the 45 mg/L COD waste at the two primary coagulant levels, the residual increases from approximately 0.02 mg/L to 0.05 mg/L (p=0.005), with constant removal efficiency at >99.5%, as the iron dose increases. This could possibly indicate that there exists a threshold sulfide concentration, below which sulfide removal is easily achieved but competition for sulfide removal from other ions or organics might be maximized at a COD concentration of 45 mg/L.

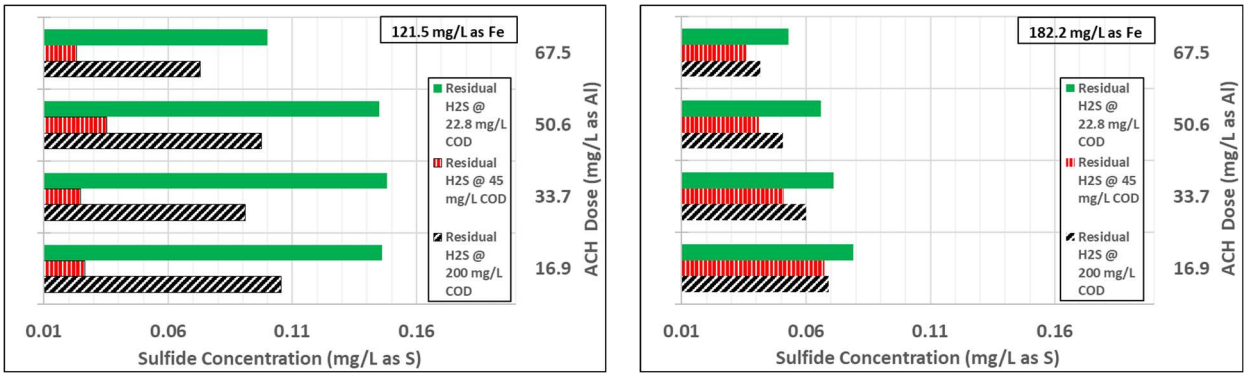

a) b)

Figure 2.2 Residual sulfide concentrations at various coagulant doses. The initial sulfide values in **Figure 2 (a)** for 22.8, 45, and 200 mg/L COD at a ferric chloride concentration of 121.5 mg/L as Fe are 31.6, 26.6, and 28.0 mg/L as S, respectively. The initial sulfide values in **Figure 2 (b)** for 22.8, 45, and 200 mg/L COD at a ferric chloride concentration of 182.2 mg/L as Fe are 28.3, 28.0, and 26.7 mg/L as S, respectively.

There is not a clear trend between an increase or decrease in COD concentration and sulfide removal. However, as shown in **Figure 2.2**, there appears to be an optimal removal of sulfide at a concentration of 45 mg/L COD. At the lower ferric chloride dose of 121.5 mg/L as Fe, increasing the COD from 45 to 200 mg/L significantly increased the residual sulfide concentration ($p < 0.001$) from an average effluent residual of 0.027 mg/L to 0.126 mg/L, and decreasing the COD from 45 mg/L to 22.8 mg/L further significantly increased residual sulfide concentration ($p = 0.008$) from an average of 0.027 mg/L to 0.225 mg/L. While the p values show that this finding cannot be

discarded, further replicability of the experiments is needed to analyze the reasons for this trend. Changing the COD concentration from 22.8 to 45 and 45 to 200 mg/L at the higher ferric chloride concentration did not cause statistically significant effects, however the same trend can still be observed in **Figure 2.2**. This could be due to the excess iron increasing the efficiency of sulfide removal at any given concentration of organics.

2.3.1.4 Settleability and Turbidity Removal

The effectiveness of ACH as a coagulant aid was also shown in these jar tests. Turbidity was shown to decrease with increases in the ACH dose in **Figure 2.3**, as settleability increases. Meanwhile, $FeCl_3$ dose increase had little impact on the turbidity, illustrating the need for a coagulant aid. The COD of the waste also influenced settleability, with higher turbidity values seen at higher COD levels. This was accompanied by an increase in phosphorus removal with increasing ACH dose, as shown in the surface plots in **Figure 2.1 a, b,** and **c**.

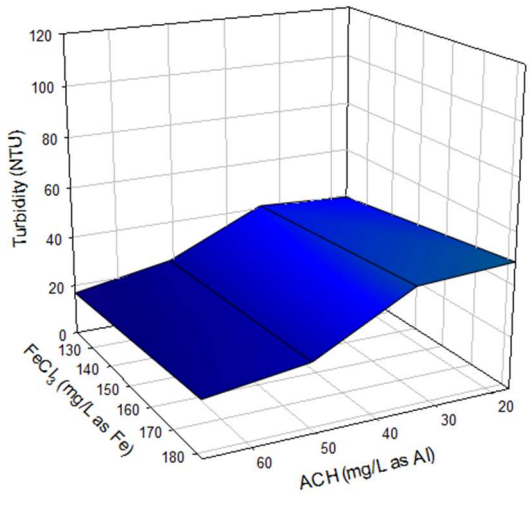

a) 22.8 mg/L COD

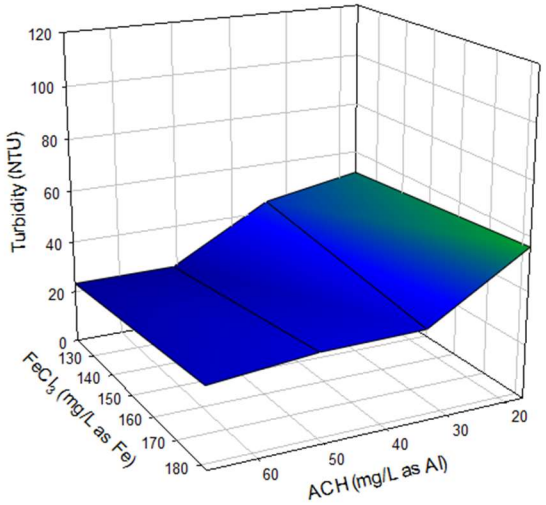

b) 45 mg/L COD

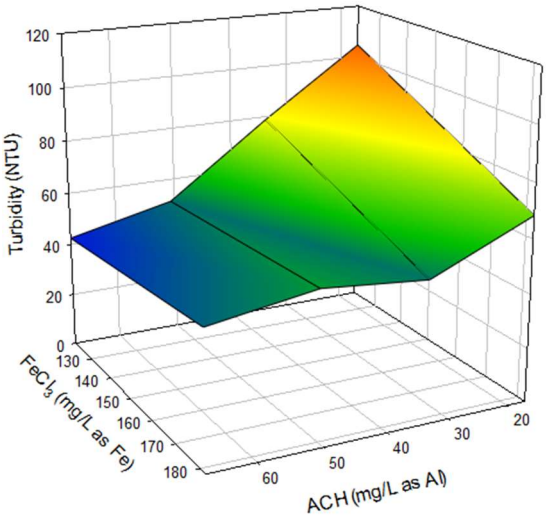

c) 200 mg/L COD

Figure 2.3 Post settling turbidity in NTU as a function of coagulants FeCl3 and ACH for bench scale jar tests with synthetic permeate, for each COD concentration.

2.3.1.5 pH Effects

A correlation between decreasing pH after the coagulation process and the residual dissolved iron can be observed in **Figure 2.4**. This is a well-known relationship from iron chemistry (U.S. Department of the Interior, 1962). In drinking water systems, iron coagulation has an operating range at pH levels between 5 and 8.5 (Crittenden and Harza, 2012). Since the pH decreases with increasing iron dose, there will be an upper bound on the ferric chloride dose that will increase precipitation of the phosphate and sulfide present without moving the pH below the operating range. The optimal pH of the permeate for precipitation would be at the higher end of the operating range, as the minimum solubility of ferric species occurs at a pH of 8.0 (Crittenden and Harza, 2012).

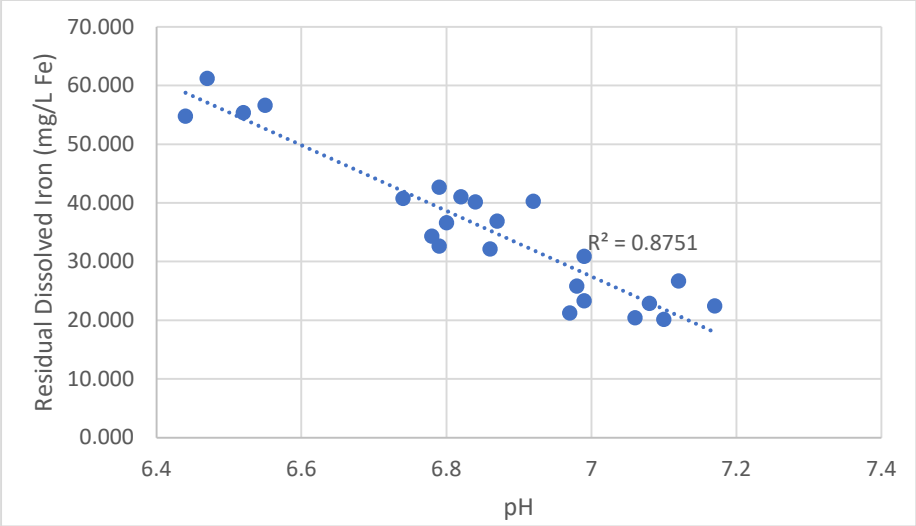

Figure 2.4 Residual iron in mg/L as Fe as a function of pH for each combination of COD and coagulant concentration tested in the synthetic permeate jar tests. Residual iron concentrations and pH were measured at the conclusion of bench scale synthetic permeate jar testing.

2.3.2 Fort Riley AnMBR Pilot Plant

2.3.2.1 Jar Testing with AnMBR Permeate

The increased phosphorus removal efficiency at the 182.2 mg/L Fe dose compared to the lower Fe doses was further confirmed from jar testing using the actual AnMBR permeate, as shown in **Figure 2.5 a).** However, the phosphorus removal efficiency is still well short of the 90% goal at either iron concentration, when the COD of the permeate was at a high value of 241 mg/L. Jar testing was then performed to find if the phosphorus recovery would increase at lower COD levels, which indeed indicated P removals above 90% for the lower COD values, especially below 140 mg/L, as shown in **Figure 2.5 b).** Increasing the COD from 120 mg/L to 241 mg/L decreased the phosphorus removal by over 15%. This decreased phosphorus removal efficiency is believed to be caused by organics complexing with phosphates, as previously discussed (Inskeep & Silvertooth, 1988; Omoike & vanLoon, 1999). Preliminary jar testing to evaluate coagulant dosing to achieve

sulfide removal alone was not conducted, as sulfide removal using ferric chloride is already well established (Gutierrez et al., 2010; Haaning Nielsen et al., 2005; Yang & Bae, 2014).

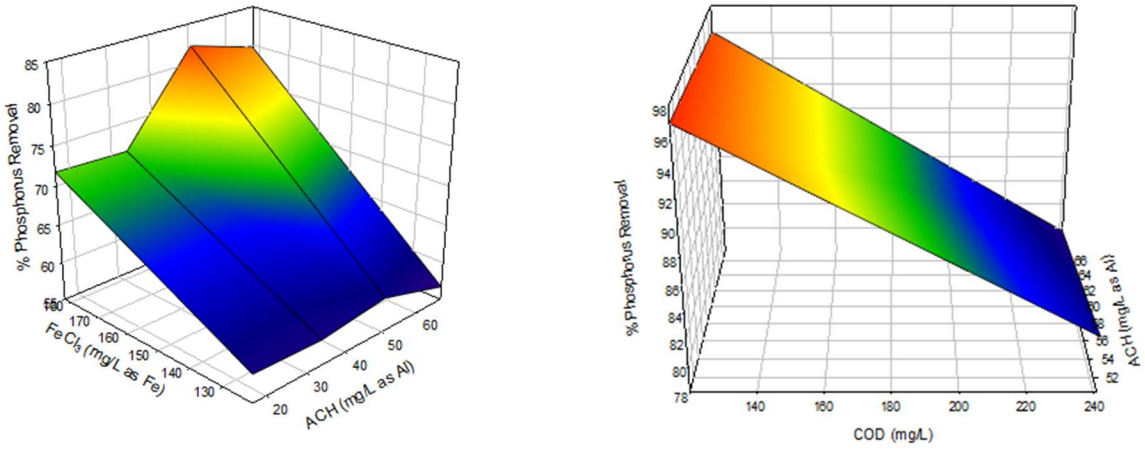

a) b)

Figure 2.5 Phosphorus removal efficiency from jar testing with actual AnMBR permeate. Panel a) shows increased phosphorus removal with increase in concentrations of the coagulants ferric chloride and ACH at 241 mg/L COD Panel b) shows the decrease of phosphorus removal with increasing COD concentration, at a fixed iron dose of 182.2 mg/L.

2.3.2.2 AnMBR Pilot Plant Continuous Operation and Effluent Water Quality

The coagulation-flocculation-sedimentation (CFS) unit integrated with the pilot scale gas sparged AnMBR began to operate successfully and continuously for a three-month period towards the end of long-term operation (Evans et al., 2018). Data obtained from the pilot AnMBR plant supports the bench scale jar tests results: total phosphorus decreased from 4.2 ± 0.6 mg/L to 0.72 ± 0.36 mg/L and the sulfide concentration decreased from 27 ± 5 to 0.7 ± 1.7 mg/L through the CFS unit (Lim et al., 2019). It should be noted that this aforementioned phosphorus removal for the CFS system is only 83%, which is less than the project goal of 90%. However, this project goal was established for removing phosphorus throughout the entire pilot plant treatment train, and not solely the CFS unit. It was discovered early on in continuous operation that abiotic phosphorus

removal occurs in the AnMBR prior to the CFS unit, with phosphorus concentrations decreasing from 7.0 ± 2.9 mg/L in the influent to 4.2 ± 0.6 mg/L in the permeate (Lim et al., 2019). Consequently, the coagulant doses were decreased from the bench scale jar test concentrations to 110 mg/L Fe and 30 mg/L Al for the lower quantum of phosphorus to be recovered in the CFS unit, further decreasing chemical costs. These decreasing phosphorus concentrations at the influent, membrane permeate, and effluent of the CFS system, throughout the operation of the AnMBR, can be seen in **Figure 2.6 a).** All total phosphorus effluent levels from the CFS unit during continuous operation met the 1.5 mg/L discharge limit, which has been proposed as a technology-based standard by the Kansas Surface Water Nutrient Reduction Plan (Kansas Department of Health and Environment, 2014). These effluent phosphorus concentrations are also similar to the discharge from a Biological Nutrient Removal (BNR) facility, which have a limit of technology (LOT) at 0.1 mg/L but typically discharge at a concentration close to 1 mg/L TP or below (U.S. EPA, 2007). Sulfide was nearly always removed at or above 99% efficiency, but the 0.1 mg/L residual goal was not always met, with an average residual concentration of 0.7 mg/L, as mentioned previously (Lim et al., 2019).

The COD effects studied in bench scale jar tests with synthetic permeate were generally in agreement with data from continuous operation of the AnMBR. As shown in **Figure 2.6 b),** during continuous operation, the phosphorus removal efficiency generally dropped with increased COD concentration, while the sulfide removal efficiency showed little impact.

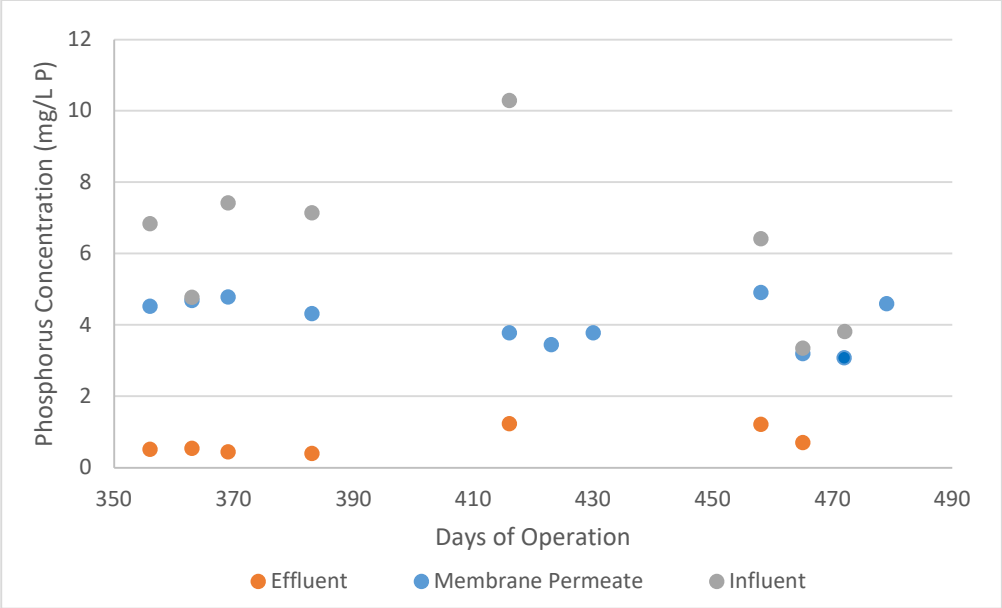

a)

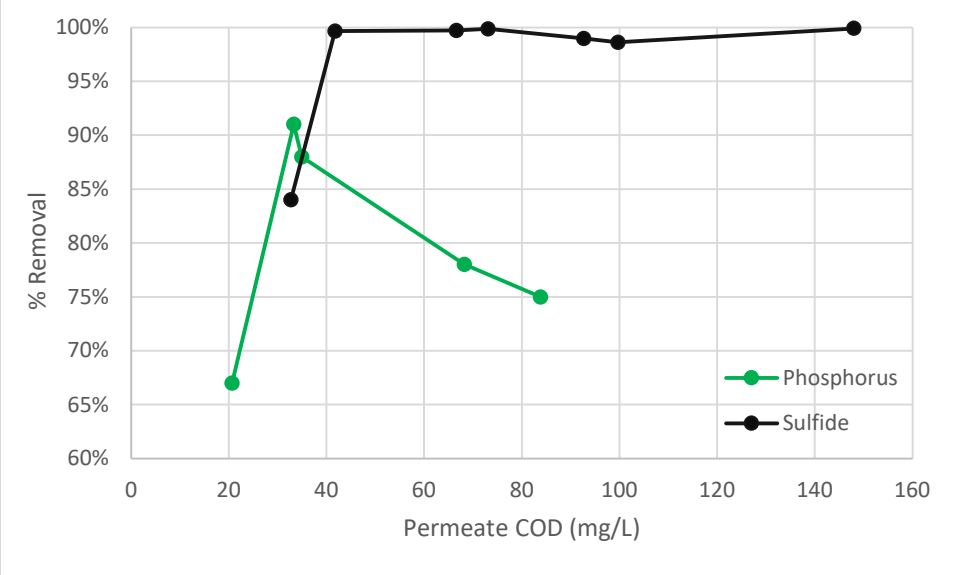

b)

Figure 2.6 a) Permeate and effluent phosphorus concentrations throughout the operation of the CFS system from day 356 of AnMBR operation to day 479. b) Phosphorus and sulfide removal by the CFS unit at various COD concentrations during continuous operation of pilot scale gas-sparged AnMBR.

2.3.3 Recovered Nutrient Product Characterization and Plant Uptake Potential

The major and trace elemental composition of the freeze-dried product collected during continuous AnMBR pilot CFS operation is provided in **Table 2.2** This product was rich in iron, aluminum, and sulfur, comprising approximately 19%, 20%, and 15%, respectively. Significant amounts of Al and Fe in these RNPs are predominantly from the iron and aluminum salts used for phosphorus precipitation in the CFS unit, which settled a product with 2.58% P. The selected trace elements concentrations in the freeze-dried product, as shown in **Table 2.2**, were low for this RNP. There are regulations and demands for fertilizer quality, efficiency, and composition, for each country (Breckenridge, 1998). According to these regulations, the quality of fertilizers is understood as the maximum allowed concentration of contaminants and desired phosphorus content and its plant availability.

Table 2.2 Selected elemental composition of the RNP obtained from the CFS unit during continuous pilot-scale AnMBR operation treating domestic wastewater.

Major Elements		Trace Elements	
Element †	Concentration% (w/w)	Element ‡	Concentration (mg/kg)
P	2.58±0.04	Zn	16.82±0.38
Al	19.29±0.17	Mo	7.17±0.03
Ca	0.42±0.00	Cd	0.04±0.00
Fe	20.17±0.38	Pb	2.06±0.05
Mg	0.07±0.01	Cr	34.27±2.01
Na	0.18±0.00	B	4.15±0.85
K	0.09±0.00	As	9.01±1.18
S	15.03±0.18	Cu	33.55±1.73

† measured using ICP-OES ‡ measured using ICP-MS

Based on the XRD analysis shown in **Figure 2.7**, it appears that there are no identifiable diffraction lines for the RNP used for the incubation study. To have identifiable peaks in an XRD, there should be at least 2% (w/w) of relevant solid species in crystalline form. According to Stratful et al. (2001), increased retention time are associated with larger recovered crystals. This was especially true for complex wastewater matrices, where organic matter or other ions could interfere with crystallization by blocking crystal growth sites and delaying crystal formation (Massey et al., 2010). As shown in **Figure 2.7** below, the XRD obtained from a different batch of the same RNP has peak positions indicating that calcite ($CaCO_3$) is prominent and iron phosphates and aluminum oxides were present with lower peak intensities. The physical and chemical differences between products can be linked to the conditions of their formation (Massey et al., 2010).

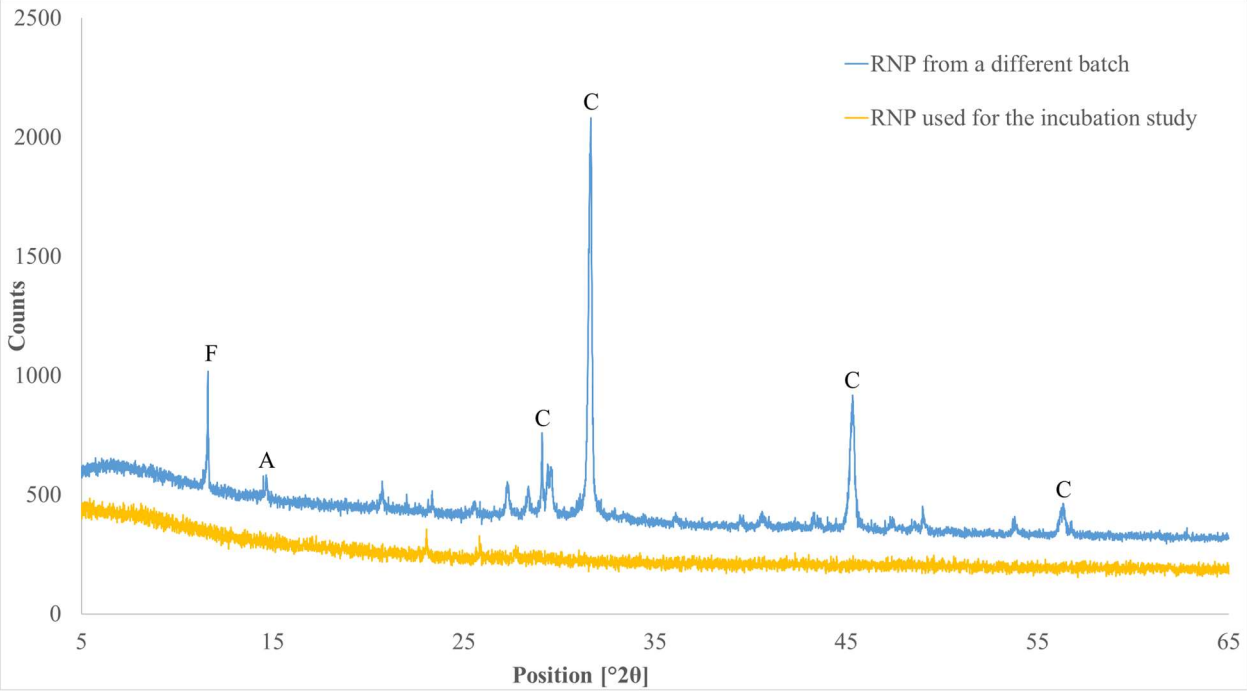

Figure 2.7 XRD patterns for selected RNP samples. A, Al (hydroxide; C, calcite; F, Fe phosphate (samples collected from days 326 and 487 of pilot plant operation)

Figure 2.8 shows the data collected from the backscattered electron (BSE) images-Energy dispersive X-ray (EDX) analyzer. The atomic number sensitivity of BSE SEM images resulting in

bright and less bright areas can be exploited to distinguish particles with different chemical composition and the EDX allows to get the elemental composition. The particles had an irregular, small, and homogeneous nature. According to the EDX of a selected particle of the RNP, the background is rich in Al (**Figure 2.8b**) and the bright colored spots rich in S which could be elemental S (**Figure 2.8e**). This coincides with the elemental composition obtained from the ICP-OES.

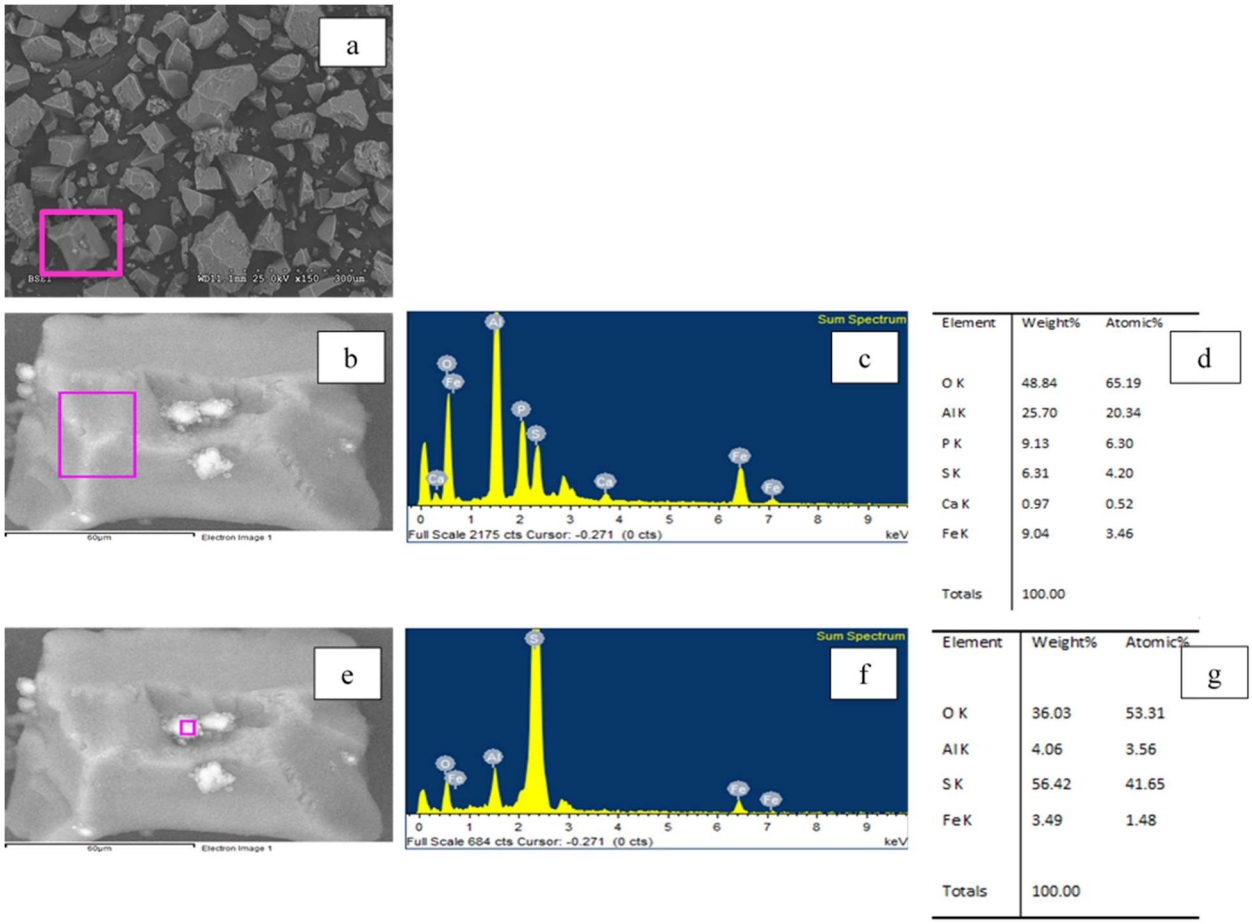

Figure 2.8 (a) Backscattered electron (BSE) image of the RNP sample used for the incubation study. Area where selected to zoom in more is outlined in pink (b) More zoomed BSE image of the background of RNP sample. Area where the elemental analysis was conducted is outlined in pink (c) Elemental composition (d) Table of elemental composition (e) Zoom-in BSE image of the bright colored area of RNP sample. Area where the elemental analysis was conducted is outlined in pink (f) Elemental composition of the selected bright colored area (g) Table of elemental composition of the selected area

X-ray absorption near-edge structure spectroscopy analysis (XANES) of the RNP sample (**Figure 2.9**) provides further evidence that this product is rich in iron adsorbed-P, such as goethite sorbed-P, and vivianite-like P. This result confirms the composition of this RNP. The lack of pre-edge suggests that these P solids do not have a well-defined crystalline structure, which supports the results of XRD analysis.

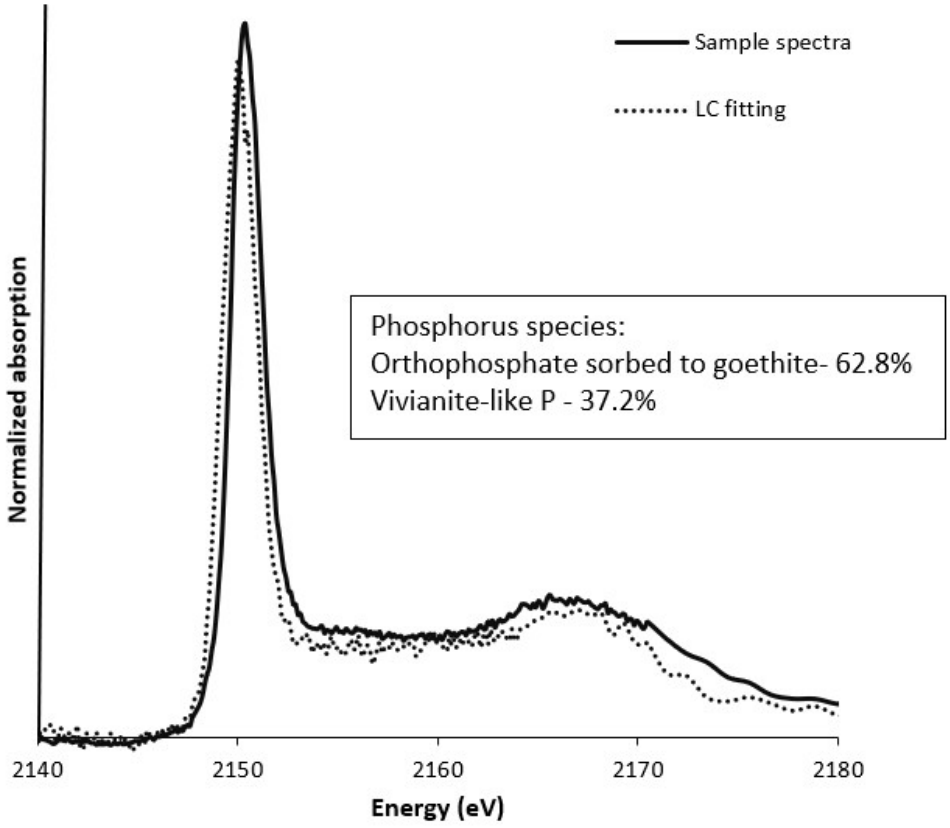

Figure 2.9 Normalized Phosphorus K-edge XANES spectra with results of linear combination (LC) fitting for RNP used in incubation study.

The soil used for the incubation study showed that the initial soil displayed characteristics of a mildly calcareous soil. Resin extractable P is a measure for potential plant available P concentration in soils (Myers et al., 2005). The greatest values of PRP were found within the 0- to 7.5mm section followed by 7.5-13.5-,13.5- to 25- and 25- to 43.5-mm sections for MAP and TSP

added treatments, as shown in **Figure 2.10**. Recovered nutrient product amended treatment showed significantly lower PRP than control for the 0-7.5 mm section followed by similar PRP as control for all other sections. **Figure 2.10** shows that soil pH significantly decreased with P treatment relative to controls at the 0-7.5 mm section for MAP and TSP. Decrease in the pH of MAP compared to control is a result of acidification due to nitrification of ammonium-N contained within the phosphorus fertilizers (Hanson & Westfall, 1985). However, this reaction was limited by the overall buffering capacity of the soil carbonates (Hettiarachchi, 2010; Lombi et al., 2004). This likely causes more PRP in the 0-7.5 mm section in MAP than the other treatments.

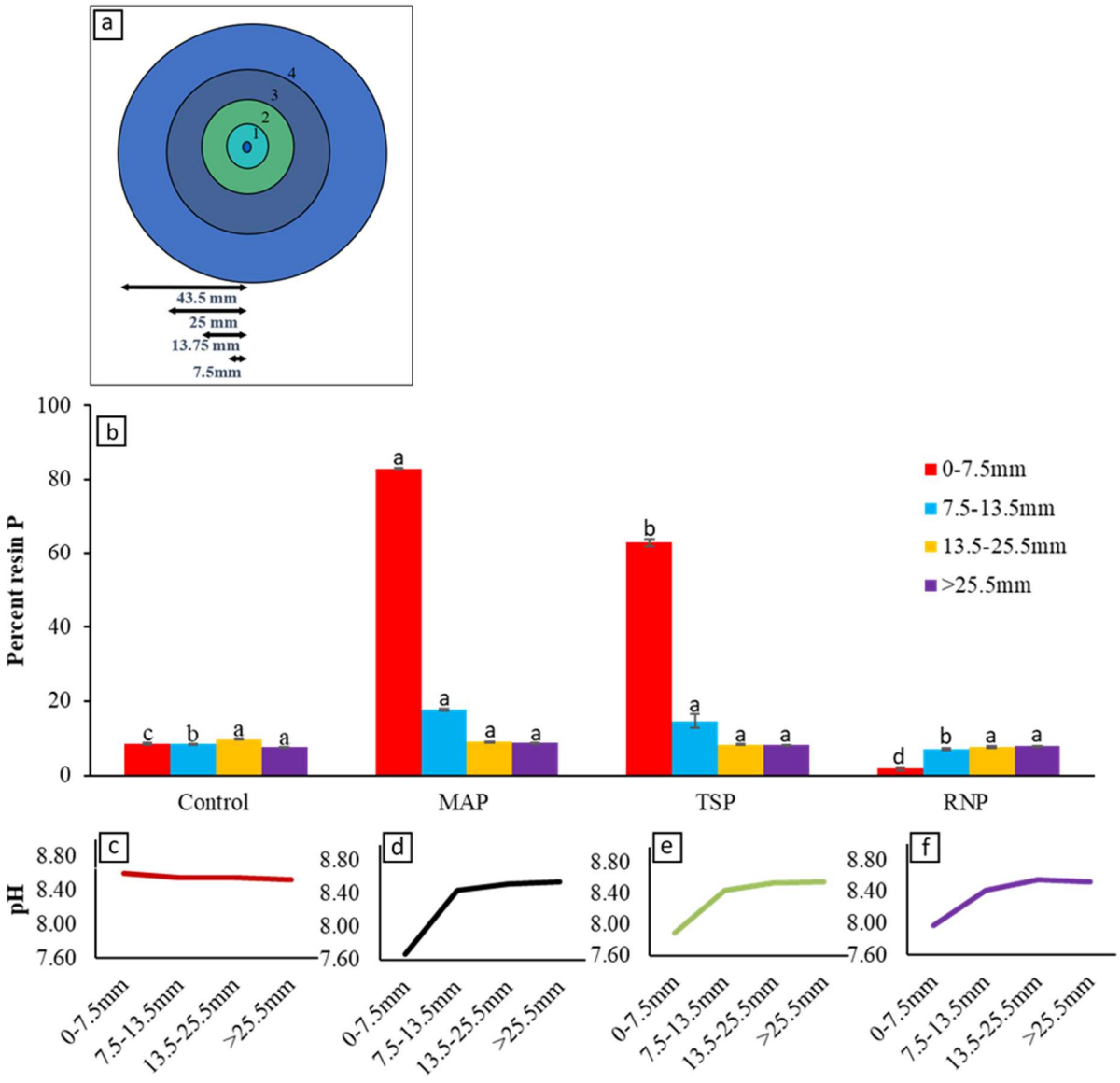

Figure 2.10 (a) Illustration of soil sections in a petri dish in the incubation study (b) Percentage of resin P (PRP) for each dish section for all treatments. Standard error bars were averaged from the four replications for each dish section. Means within a soil section for each treatment containing the same letter are not significantly different at p = 0.05 according to Least significant difference method. MAP, monoammonium phosphate; TSP, triple superphosphate; RNP, recovered nutrient product (c) pH for each dish section for control (d) pH for each dish section for MAP (e) pH for each dish section for TSP (f) pH for each dish section for RNP.

The phosphorus availability in calcareous soils is determined by phosphate adsorption and precipitation reactions with calcium carbonate. Dissolution of TSP causes direct soil acidification

(Lindsay, 1979). Triple superphosphate, which contains monocalcium phosphate [$Ca(H_2PO_4)_2 \cdot H_2O$], dissociates H^+ ion from the $H_2PO_4^-$ molecule and generates acidity. This leads to higher PRP in the 0-7.5 mm section in TSP than the RNP and control. Due to the indirect nature of soil acidification by MAP, it could persist for a longer time than TSP. The RNP was able to buffer the soil pH at its original pH. Presence of iron and aluminum oxides, which facilitate the sorption of phosphorus in soil, reduces the available phosphorus for plants. Aluminum or iron oxide-containing drinking water treatment residuals have been beneficially used as a Best Management Practice (BMP) to remove dissolved phosphorus from agricultural runoff water and therefore to enhance the surface water quality (Dayton et al., 2003). According to Novak & Watts (2004), application of water treatment residues (WTR) reduces the extractable soil P concentrations in a soil with excessive P concentrations and decreases the amount of P available for off -site transport. Applications of WTR with higher phosphorus sorption maximum values could be a part of a best management practice for biosolids or manure field applications (Ippolito et al., 2011). This product also shows a reduction of plant available P after application and therefore can be used as a P sink for this tested soil. In coastal sediments, previous studies have also shown that iron phosphates, including vivianite, act as phosphorus sinks (Beauchemin et al., 2003; Dijkstra et al., 2014; Egger et al., 2015; Weeks & Hettiarachchi, 2020). This indicates that vivianite recovery from wastewater may likely not lead to an effective fertilizer product despite growing interest motivated by the desire for an alternative to struvite recovery that has simpler process operation and does not require EBPR (Wilfert et al., 2018; Wu et al., 2019), as well as work showing it may be more efficiently separated from sludge than struvite (Wilfert et al., 2018). However, the reduced availability of P in the captured P-rich RNP could be beneficial in several

other scenarios where excess phosphorus runoff could lead to huge ecosystem impacts such as eutrophication, harmful algal blooms, and hypoxic zones in surface waters.

2.4 Conclusions

Bench scale jar testing with synthetic and actual AnMBR permeate has demonstrated that a variety of factors, including the coagulant and coagulant aid concentration, the pH of the permeate, and the permeate COD concentration, determines the optimum coagulant dosing in a system where phosphate and sulfide are both present. There is a threshold to the sulfide removal that can be economically achieved, and an increased iron dose can even decrease the sulfide removal efficiency at high enough Fe levels. To achieve the highest phosphorus removal, iron dosage is the limiting factor due to the preferential precipitation of sulfide over phosphate. An increased presence of organic COD can increase the iron dosage required even further. Due to settleability issues in anaerobic systems, the addition of aluminum chlorohydrate (ACH) as a coagulant aid was necessary. This study demonstrated that ACH increased settleability and decreased turbidity, in addition to aiding phosphorus removal and thus decreasing ferric iron demand. The bench scale results were successfully verified in a pilot scale coagulation-flocculation-sedimentation (CFS) system downstream of a gas sparged AnMBR with consistent removals of phosphorus and sulfide at or above 90% and 99%, respectively. The pilot system also confirmed that increasing permeate COD concentration decreased phosphorus removal efficiency but had little to no impact on the sulfide removal efficiency. Detailed and novel soil characterization studies on the RNPs from the CFS unit demonstrated that P-rich RNPs may not be an effective slow-release fertilizer product as widely perceived in recent literature, rather they likely act as a phosphorus sink in agricultural systems, which could be a beneficial application in of itself in certain scenarios, especially

pertaining to preventing eutrophication of water bodies from land applied phosphorus in phosphorus rich soils.

2.5 Acknowledgements

I would like to thank Ms. Kasuni Gamage for her work on the soil characterization and plant uptake sections in this chapter of the thesis, which is a manuscript published in the journal, *Science of the Total Environment*.

2.6 References

Allison, L. E. and Moodie, C. D. (1965). Carbonate. In C.A. Black et al. (ed.) Methods of soil analysis Part 2, 2nd ed. *Agron. Monogr*. 9, p. 1379-1400. ASA, CSSA, and SSSA, Madison, WI, 1965.

Beauchemin, S., Hesterberg, D., Chou, J., Beauchemin, M., Simard, R. R., & Sayers, D. E. (2003). Speciation of Phosphorus in Phosphorus-Enriched Agricultural Soils Using X-Ray Absorption Near-Edge Structure Spectroscopy and Chemical Fractionation. *Journal of Environmental Quality*, *32*(5), 1809–1819. https://doi.org/10.2134/jeq2003.1809

Breckenridge, R. P. (1998). Determination of Background Concentrations of Inorganics in Soils and Sediments at Hazardous Waste Sites. *Environmental Monitoring and Assessment*, *51*(3), 621–656.

Caravelli, A. H., Contreras, E. M., & Zaritzky, N. E. (2010). Phosphorous removal in batch systems using ferric chloride in the presence of activated sludges. *Journal of Hazardous Materials*, *177*(1), 199–208. https://doi.org/10.1016/j.jhazmat.2009.12.018

Dayton, E.A., Basta, N. T., Jakober, C.A., and Hattey, J.A. (2003). Using treatment residuals to reduce phosphorous in agricultural runoff. *J. Am. Water Works Assoc.*, 95, 151–158.

Dijkstra, N., Kraal, P., Kuypers, M. M. M., Schnetger, B., & Slomp, C. P. (2014). Are iron-phosphate minerals a sink for phosphorus in anoxic Black Sea sediments? *PloS One*, *9*(7), e101139–e101139. https://doi.org/10.1371/journal.pone.0101139

Egger, M., Jilbert, T., Behrends, T., Rivard, C., & Slomp, C. P. (2015). Vivianite is a major sink for phosphorus in methanogenic coastal surface sediments. *Geochimica et Cosmochimica Acta*, *169*, 217–235. https://doi.org/10.1016/j.gca.2015.09.012

Gutierrez, O., Park, D., Sharma, K. R., & Yuan, Z. (2010). Iron salts dosage for sulfide control in sewers induces chemical phosphorus removal during wastewater treatment. *Water Research (Oxford)*, *44*(11), 3467–3475. https://doi.org/10.1016/j.watres.2010.03.023

Haaning Nielsen, A., Lens, P., Vollertsen, J., & Hvitved-Jacobsen, T. (2005). Sulfide–iron interactions in domestic wastewater from a gravity sewer. *Water Research (Oxford)*, *39*(12), 2747–2755. https://doi.org/10.1016/j.watres.2005.04.048

Hanson, R. L., & Westfall, D. G. (1985). Orthophosphate solubility transformations and availability from dual applied nitrogen and phosphorus. *Soil Science Society of America Journal*, *49*(5), 1283–1289. https://doi.org/10.2136/sssaj1985.03615995004900050043x

Hatton, W., & Simpson, A. M. (1985). Use of alternative aluminium based chemicals in coagulation with particular reference to phosphorus removal. *Environmental Technology Letters*, *6*(1–11), 225–230. https://doi.org/10.1080/09593338509384339

Hettiarachchi, G. M. (2010). Chemical behavior of fluid and granular Mn and Zn fertilisers in alkaline soils. *Australian Journal of Soil Research*, *48*(3), 238–247.

Inskeep, W. P., & Silvertooth, J. C. (1988). Inhibition of hydroxyapatite precipitation in the presence of fulvic, humic, and tannic acids. *Soil Science Society of America Journal*, *52*(4), 941–946. https://doi.org/10.2136/sssaj1988.03615995005200040007x

Ippolito, J. A., Barbarick, K. A., & Elliott, H. A. (2011). Drinking Water Treatment Residuals: A Review of Recent Uses. *Journal of Environmental Quality*, *40*(1), 1–12. https://doi.org/10.2134/jeq2010.0242

Jenkinson, D. S., & Powlson, D. S. (1976). The effects of biocidal treatments on metabolism in soil—V: A method for measuring soil biomass. *Soil Biology & Biochemistry*, *8*(3), 209–213. https://doi.org/10.1016/0038-0717(76)90005-5

Kilmer, V. J., & Alexander, L. T. (1949). Methods of making mechanical analyses of soils. *Soil Science*, *68*(1), 15–24. https://doi.org/10.1097/00010694-194907000-00003

Lim, K., Evans, P. J., & Parameswaran, P. (2019). Long-Term Performance of a Pilot-Scale Gas-Sparged Anaerobic Membrane Bioreactor under Ambient Temperatures for Holistic Wastewater Treatment. *Environmental Science & Technology*, *53*(13), 7347–7354. https://doi.org/10.1021/acs.est.8b06198

Lindsay, W. L. (1979). *Chemical equilibria in soils*. Wiley.

Lombi, E., McLaughlin, M. J., Johnston, C., Armstrong, R. D., & Holloway, R. E. (2004). Mobility and lability of phosphorus from granular and fluid monoammonium phosphate differs in a calcareous soil. *Soil Science Society of America Journal*, *68*(2), 682–689. https://doi.org/10.2136/sssaj2004.0682

Massey, M. S., Ippolito, J. A., Davis, J. G., & Sheffield, R. E. (2010). Macroscopic and microscopic variation in recovered magnesium phosphate materials: Implications for phosphorus removal processes and product re-use. *Bioresource Technology*, *101*(3), 877–885. https://doi.org/10.1016/j.biortech.2009.08.110

Murphy, J., & Riley, J. P. (1962). A modified single solution method for the determination of phosphate in natural waters. *Analytica Chimica Acta*, *27*(C), 31–36. https://doi.org/10.1016/S0003-2670(00)88444-5

Myers, R. G., Sharpley, A. N., Thien, S. J., & Pierzynski, G. M. (2005). Ion-Sink Phosphorus Extraction Methods Applied on 24 Soils from the Continental USA. *Soil Science Society of America Journal*, *69*(2), 511–521. https://doi.org/10.2136/sssaj2005.0511

Nelson, D. W. and Sommers, L. E. (1996). Total carbon, organic carbon, and organic matter. In: D.L. Sparks, A. Page, P. Helmke, R. Loeppert, P. Soltanpour, M. Tabatabai, et al., editors, Methods of soil analysis Part 3 Chemical methods, ASA, CSSA, SSSA. Madison, WI.

Novak, J. M., & Watts, D. W. (2004). Increasing the phosphorus sorption capacity of southeastern Coastal Plain soils using water treatment residuals. *Soil Science*, *169*(3), 206–214. https://doi.org/10.1097/01.ss.0000122522.03492.30

Olsen, S. R. (1954). *Estimation of available phosphorus in soils by extraction with sodium bicarbonate*. USDeptof Agriculture.

Omoike, A. I., & vanLoon, G. W. (1999). Removal of phosphorus and organic matter removal by alum during wastewater treatment. *Water Research (Oxford)*, *33*(17), 3617–3627. https://doi.org/10.1016/S0043-1354(99)00075-5

Pierzynski, J., & Hettiarachchi, G. M. (2018). Reactions of Phosphorus Fertilizers with and without a Fertilizer Enhancer in Three Acidic Soils with High Phosphorus-Fixing Capacity. *Soil Science Society of America Journal*, *82*(5), 1124–1139. https://doi.org/10.2136/sssaj2018.01.0064

Ravel, B., & Newville, M. (2005). ATHENA, ARTEMIS, HEPHAESTUS: Data analysis for X-ray absorption spectroscopy using IFEFFIT. *Journal of Synchrotron Radiation*, *12*(4), 537–541. https://doi.org/10.1107/S0909049505012719

SAS Institute. (2011). The SAS system for Windows version 9.1.3, SAS Institute, Cary, NC.

Soil Survey Laboratory Staff. (2004). Soil survey methods manual. Soil survey investigations Rep. No. 42 Version 4.0. National Soil Survey Center. Lincoln, NE.

Soil Survey Staff. (2011). Soil Survey Investigations Report No. 45. Version 2.0. R. Burt (ed.). *Soil Survey Laboratory Information Manual.* U.S. Department of Agriculture, Natural Resources Conservation Service.

Stratful, I., Scrimshaw, M. D., & Lester, J. N. (2001). Conditions influencing the precipitation of magnesium ammonium phosphate. *Water Research (Oxford)*, *35*(17), 4191–4199. https://doi.org/10.1016/S0043-1354(01)00143-9

Wang, Y., Tng, K. H., Wu, H., Leslie, G., & Waite, T. D. (2014). Removal of phosphorus from wastewaters using ferrous salts—A pilot scale membrane bioreactor study. *Water Research (Oxford)*, *57*, 140–150. https://doi.org/10.1016/j.watres.2014.03.029

Watson, M. E. and Brown, J.R. (1998). pH and lime requirement. In: J.R. Brown, editor, Recommended chemical soil test procedures for the north central region. Missouri Agric. Exp. Stn, Univ. of Missouri, Columbia, MO. p. 13–16.

Weeks, J. J., & Hettiarachchi, G. M. (2020). Source and formulation matter: New insights into phosphorus fertilizer fate and transport in mildly calcareous soils. *Soil Science Society of America Journal*, *84*(3), 731–746. https://doi.org/10.1002/saj2.20054

Werner, F., & Prietzel, J. (2015). Standard Protocol and Quality Assessment of Soil Phosphorus Speciation by P K-Edge XANES Spectroscopy. *Environmental Science & Technology*, *49*(17), 10521–10528. https://doi.org/10.1021/acs.est.5b03096

Wilfert, P., Dugulan, A. I., Goubitz, K., Korving, L., Witkamp, G. J., & Van Loosdrecht, M. C. M. (2018). Vivianite as the main phosphate mineral in digested sewage sludge and its role for

phosphate recovery. *Water Research (Oxford)*, *144*, 312–321. https://doi.org/10.1016/j.watres.2018.07.020

Williams, R. F. (1948). The Effects of Phosphorus Supply on The Rates of Intake of Phosphorus and Nitrogen and Upon Certain Aspects of Phosphorus Metabolism in Gramineous Plants. *Australian Journal of Biological Sciences*, *1*(3), 333-. https://doi.org/10.1071/BI9480333

Wu, Y., Luo, J., Zhang, Q., Aleem, M., Fang, F., Xue, Z., & Cao, J. (2019). Potentials and challenges of phosphorus recovery as vivianite from wastewater: A review. *Chemosphere (Oxford)*, *226*, 246–258. https://doi.org/10.1016/j.chemosphere.2019.03.138

Yang, S., & Bae, J. (2014). A feasibility of coagulation as post-treatment of the anaerobic fluidized bed reactor (AFBR) treating domestic wastewater. *Journal of the Korean Society of Water and Wastewater*, *28*(6), 623–634. https://doi.org/10.11001/jksww.2014.28.6.623

Zarcinas, B. A., McLaughlin, M. J., & Smart, M. K. (1996). The effect of acid digestion technique on the performance of nebulization systems used in inductively coupled plasma spectrometry. *Communications in Soil Science and Plant Analysis*, *27*(5/8), 1331–1354. https://doi.org/10.1080/00103629609369636

Zhou, Y., Xing, X.-H., Liu, Z., Cui, L., Yu, A., Feng, Q., & Yang, H. (2008). Enhanced coagulation of ferric chloride aided by tannic acid for phosphorus removal from wastewater. *Chemosphere (Oxford)*, *72*(2), 290–298. https://doi.org/10.1016/j.chemosphere.2008.02.028

Chapter 3 - Phosphorus Recovery by Calcium Phosphate Precipitation

3.1 Introduction

There is great potential for resource recovery from swine wastewater. The high concentration of phosphorus in the swine lagoon wastewater allows for a larger nutrient load to be precipitated as calcium phosphate recovered nutrient product (RNP). Recovering phosphorus from wastewater could be a significant component of the circular economy that reduces the burden on phosphate mineral reserves as global food production continues to grow, while simultaneously reducing nutrient pollution that can lead to harmful algal blooms and dead zones. Specifically, for farmers in southwest Kansas, capture of a calcium phosphate fertilizer product could help supplement the capital and operational costs of an AnMBR system, which by treating the wastewater at a smaller footprint, reduces the amount of land they need for storing this waste and provides them with a new source of water, an important commodity as the Ogallala aquifer continues to be depleted. Removing the phosphorus from the water is an important benefit for hog farmers in Kansas, as nutrient management is a significant hurdle for their waste management to meet regulatory requirements in their discharge. This was the driving force behind a patented phosphorus reduction system (Phred) developed with the help of the Kansas Environmental Management Association that unfortunately has never taken off (Manure Manager). There is a demand in this region for managing waste and recovering resources.

The objectives of this study are to first evaluate the required dosing of calcium oxide required to remove the large concentration of phosphorus from swine wastewater and then to evaluate how to tailor the treatment towards forming a better fertilizer product. This tailored treatment focused on how to optimize phosphorus removal, while keeping the product at a suitable pH. There is limited

work on adjusting treatment for more beneficial recovery. Sulfide removal by calcium addition was also evaluated in this study.

3.2 Materials and Methods

3.2.1 Bench Scale Jar Testing

A synthetic swine media was prepared to simulate the permeate after treatment of swine waste through the AnMBR. The media had the following composition based on previous studies of swine waste treatment: 378 mg/L NH_4-N, 342 mg/L K, 21 mg/L Mg, 39 mg/L Ca, 0.9 mg/L Fe, and a 50 mM borate buffer (Raby et al., 2013). Based on a 90% removal rate achieved in the pilot-scale gas-sparged AnMBR treating municipal wastewater (Lim et al., 2019), 1080 mg/L of COD was added to simulate a decrease from 10,000 mg/L COD of influent raw swine wastewater (Huang et al., 2015). Characterization of the swine lagoon at animal farms of Kansas State University showed typical COD concentrations lower than this, but a shock load of fresh waste can periodically lead to this high level of organic loading. The COD was added as 154.2 mg/L propionic acid, 146.4 mg/L acetic acid, 300 mg/L lactic acid, 7 mg/L butyric acid, and 170 mg/L ethanol (Huang et al., 2015). There were a few deviations from this recipe to more accurately mimic the swine lagoon wastewater composition at the K-State animal farm. 30 mg/L of dissolved sodium sulfide was also included in the media to mimic the swine wastewater, as the sulfate-reducing bacteria (SRBs) found in the reactor will reduce the sulfate from the influent to hydrogen sulfide (Damodara Kannan et al., 2020). Additionally, the phosphate concentration was decreased from 105 mg/L to 50 mg/L and the pH was adjusted to 7.5, instead of 8, by addition of sodium hydroxide, to reflect the swine lagoon characterization (Raby et al., 2013).

Once the synthetic permeate was appropriately dosed, initial conditions of dissolved calcium, total phosphorus, sulfide, and pH were recorded. The pH of the permeate was increased to the appropriate level for each experiment using 5 M sodium hydroxide.

The coagulant was then added to four beakers filled with 1000 mL of the synthetic permeate. The beakers were then rapidly mixed at 100 RPM for two minutes, after which the mixing speed was reduced to 30 RPM for 20 minutes. The jars were mixed using a Phipps & Bird Stirrer (model 7790-400). Once the slow mixing was completed, the contents of each jar were placed in 1000 mL graduated cylinders to settle for 30 minutes to evaluate sludge settleability. Once settleability was assessed, a sample was collected from the top two inches of the graduated cylinder and tested for turbidity. A liquid sample was collected from each cylinder and filtered through a 1.2 μm GF/C filter. The filtered samples were then tested for residual sulfide, total phosphorus, and dissolved iron. The unfiltered waste in each cylinder was finally tested for pH.

3.2.2 Bench Scale Analytical Methods

Residual dissolved sulfide tests were conducted following the USEPA Methylene Blue Method (Method 8131) using a HACH DR 1900 spectrophotometer. Dissolved calcium was measured using ion chromatography (IC) analysis (Thermo Scientific, USA). HACH TNT 843 and 845 kits (concentration range 0.05 – 1.5 mg/L as P and 2 – 20 mg/L as P, respectively) were used to measure total phosphorus. COD concentrations were verified using HACH TNT 822 kits (concentration range 20-1500 mg/L). The HACH kits were analyzed using the HACH DR 3900 spectrophotometer. pH analysis was conducted using a pH analysis was conducted using a VWR sympHony B10P pH benchtop meter.

Minitab Statistical Software was used to calculate p values for determining statistical significance.

3.2.3 Calcium Oxide Coagulant Chemistry

The calcium coagulant chosen was calcium oxide, or quicklime, because it is cheap and easy to obtain in bulk. The bench scale experiments will test the phosphorus removal efficiency by varying calcium oxide at concentrations between 64 and 518 mg/L as Ca. These values were chosen based on the molar ratio of calcium added to phosphate in the permeate, ranging from a Ca/P of 1/1 to 8/1.

After developing this dosing curve from 1/1 to 8/1, an optimum dose was chosen to conduct further experiments to lower the final pH of the RNP solids, as previous work has shown that more basic fertilizers are not as soluble in soil, which will inhibit movement and uptake by plants (Kasuni Gamage, verbal communication and unpublished results; Fien Degryse et al., 2017). One of these additional tests would change the initial pH of the permeate to values from 6-7.5. The next round of batch experiments tested combinations of calcium chloride with the calcium oxide. Calcium chloride was selected because it is commonly used for calcium addition (Tran et al., 2014), and it does not release hydroxide ions when added to water as calcium oxide does.

Visual MINTEQ 3.1 was used to calculate the supersaturation indices of the different calcium phosphate species formed. Supersaturation index (SI) is calculated as the log IAP – log K_{sp} where IAP is the ion activity product and K_{sp} is the solubility product (Tran et al., 2014).

3.3 Results and Discussion

3.3.1 Phosphorus Removal from Calcium Oxide Addition

Addition of quicklime to the synthetic swine permeate forms calcium hydroxide, releasing both calcium and hydroxide ions. These ions then react with phosphate to precipitate out calcium phosphate. The hydroxide ions are important for the formation of several of the crystalline forms of calcium phosphate, as well as increasing the pH. Although some of the calcium phosphate

species form at low pH, and even hydroxyapatite can form at pH as low as 7, it has been observed empirically that higher pH increases the supersaturation index and causes calcium phosphate products to precipitate more readily (Lei et al., 2017; Tran et al., 2014; Wang & Nancollas, 2008). **Figure 3.1** illustrates that the phosphorus removal increased with increasing pH.

The ratio of calcium to phosphate is also critical to precipitation processes. As shown in **Figure 3.1**, phosphorus removal increases with increase in Ca/P ratio. The largest increases in phosphorus removal efficiency occurs between the 1/1 Ca/P ratio to 3/1 Ca/P ratio of quicklime, after which the removal efficiencies begin to level off between 90% and 98%. Although the Ca/P stoichiometric ratio necessary for calcium phosphate precipitation is between 1 and 1.67 (Raynaud et al., 2002), additional calcium addition is often needed to drive the solution to supersaturation and more readily lead to the precipitation of these desired products, and this has been shown in previous studies (Tran et al., 2014). The results from this study show this trend as well, as the phosphorus removal efficiency at coagulant doses of the stoichiometric 1/1 to 2/1 levels are quite low, between 20 and 50%.

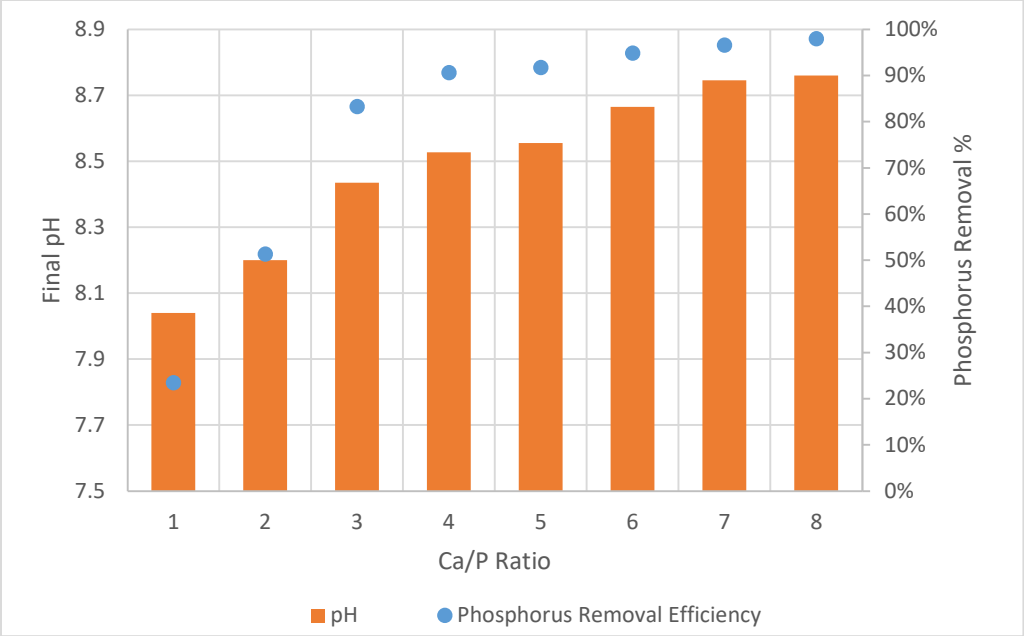

Figure 3.1 Dosing curve of phosphorus removal by calcium oxide addition from 1/1 Ca/P to 8/1 Ca/P.

Table 3.1 below provides the SI for various calcium phosphate species that would form in the given conditions, as calculated by Visual MINTEQ. Based on these indices, hydroxyapatite, octacalcium phosphate, tricalcium phosphate, monotite, and brushite all have the potential to form for each molar ratio of Ca/P. However, monotite and brushite generally form at lower pH values, and based on preliminary characterization of the products, they are not forming in this calcium RNP (Kasuni Gamage, verbal communication and unpublished results). It is possible that the kinetics of these two mineral formations or variation in solubility constants of the real RNP precipitates from these pure minerals lead to the absence of monotite and brushite in this system. The supersaturation index is an indication of the thermodynamic favorability of these precipitation reactions, and therefore it is logical that they generally increase for each product as the Ca/P increases (Tran et al., 2014). The one exception is the 4/1 ratio, where hydroxyapatite has its highest SI. This 4/1 Ca/P dose of calcium oxide seems to be an optimal point for this precipitation

process, as the phosphorus removal is at 90%, the pH is still relatively low, and the cost will be lower than at the higher removal efficiencies because of the amount of calcium oxide needed.

Table 3.3. Supersaturation Indices of potential calcium phosphate products.

Ca/P Ratio	Hydroxyapatite	Octacalcium phosphate	Tricalcium phosphate	Monotite	Brushite
1/1	14.32	4.889	4.563	0.573	0.291
2/1	15.778	5.833	5.364	0.716	0.435
3/1	17.112	6.577	6.056	0.768	0.486
4/1	19.44	6.933	6.385	0.796	0.514
5/1	18.101	7.162	6.581	0.829	0.547
6/1	18.618	7.405	6.835	0.818	0.536
7/1	18.997	7.576	7.018	0.806	0.524
8/1	19.191	7.689	7.121	0.817	0.535

3.3.1.1 pH Adjusting Experiments

The 4/1 Ca/P ratio of calcium oxide to be added was chosen as desired ratio for further optimization of the calcium phosphate precipitation system. Additional experiments were done to reduce the pH of the final product. This was motivated by previous work, which has shown that more basic fertilizers are not as soluble in soil, which will inhibit transport and uptake by plants (Kasuni Gamage, verbal communication and unpublished results; Fien Degryse et al., 2017). Two methods were tested for decreasing the pH - decreasing the initial pH of the permeate and adding calcium chloride to supplement the calcium oxide dose. It should be noted that the data for the control 4/1 Ca/P of calcium oxide addition in the data below is different than that from **Figure 3.1**. The 4/1 Ca/P addition was repeated to provide a more accurate control by subjecting this test to the same experimental conditions as the new tests.

Figure 3.2 below shows the results of adjusting the initial pH of the synthetic swine permeate. The final pH appears to be relatively stable at around 8.8 and unresponsive to step changes in initial

pH from 6 – 7.5. This is most likely due to the strong buffering capacity of the permeate likely resulting from the Calcium oxide addition. Significant improvements in pH would have been needed to pursue this option further, as controlling the pH of the permeate would be a difficult operational challenge and increased chemical expenses from hydrochloric acid addition.

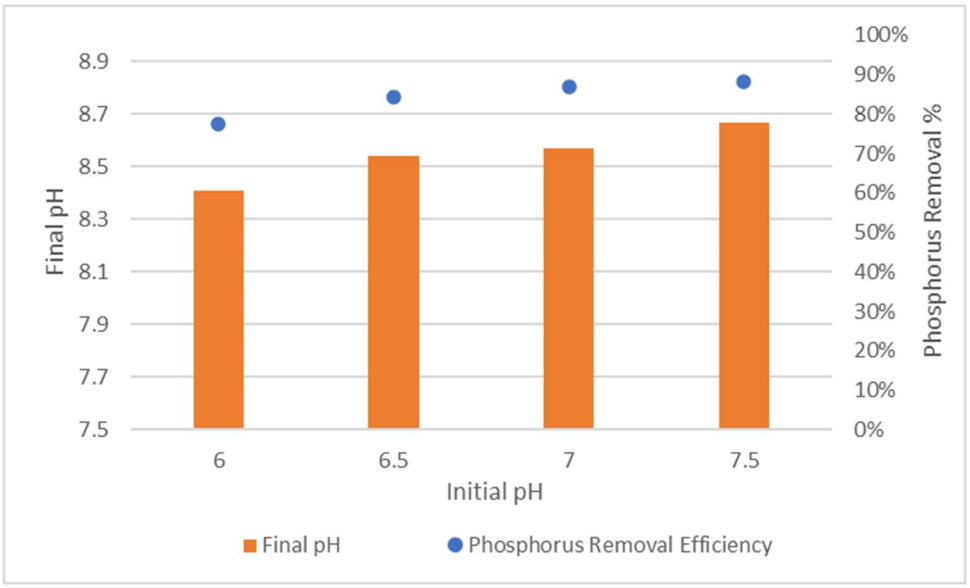

Figure 3.2 Phosphorus removal efficiency at adjusted initial permeate pH values (4/1 Ca/P ratio).

The next method considered for lowering the pH to increase soil solubility of the RNP was to add calcium chloride in combination with the calcium oxide, maintaining the same 4/1 Ca/P ratio, but decreasing the concentration of hydroxides originating from calcium oxide addition. This had some success. Both the 50/50 ratio of calcium oxide to calcium chloride and the 75/25 ratio significantly decreased the final pH from the control 4/1 ratio ($p = 0.007$ and $p = 0.05$, respectively), but they both also significantly decreased phosphorus removal ($p < 0.001$ and $p = 0.001$, respectively), as shown in **Figure 3.3** below. Additionally, it should be considered that the 75/25 ratio of calcium oxide to calcium chloride does not significantly increase phosphorus

removal from simply adding the same calcium oxide at the 3/1 Ca/P level without calcium chloride ($p = 0.223$), and it does not lower the pH. The 50/50 ratio does increase phosphorus removal significantly ($p < 0.001$ from 51% at the 2/1 Ca/P concentration to 77%. The choice of which dosing option to choose is dependent on the choice of desired outcome between phosphorus removal from wastewater or capture of a valuable product that is more soluble and available in soil is more important for the application.

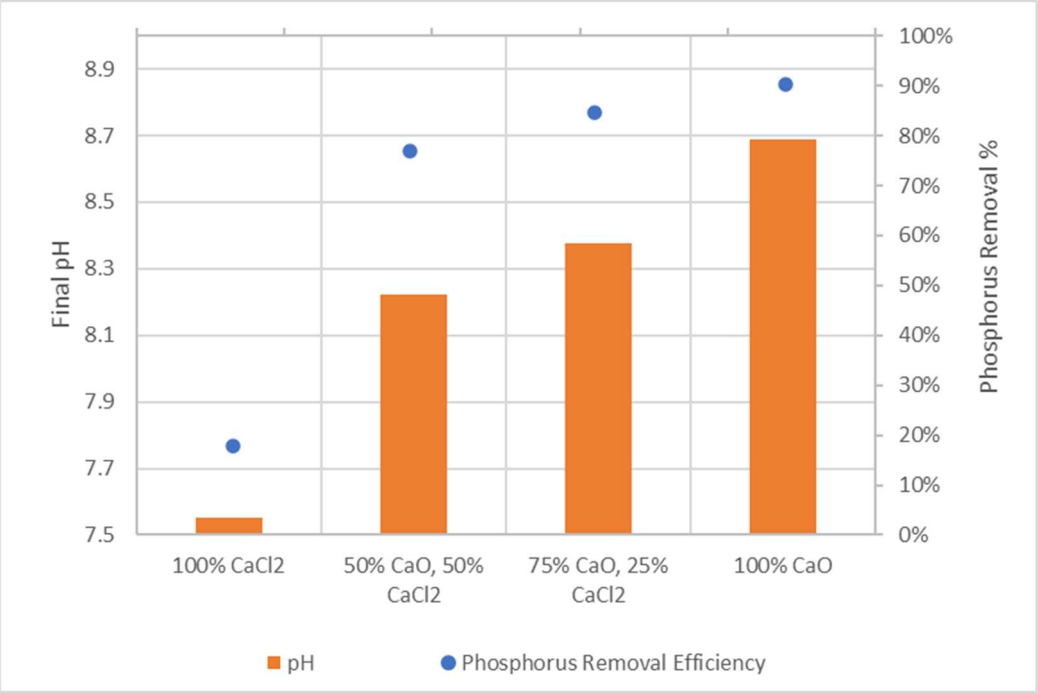

Figure 3.3 Phosphorus removal from combined dose of calcium oxide with calcium chloride (4/1 Ca/P ratio).

3.3.2 Sulfide Residual

Sulfide removal from calcium addition has not been demonstrated, which is one disadvantage of calcium precipitation compared to iron precipitation for treating AnMBR permeate with high dissolved hydrogen sulfide concentrations. From the jar testing results, this study found that the sulfide residual from the 4/1 Ca/P ratio was 26.5 mg/L as S compared to 23.4 mg/L as S from a control jar of synthetic permeate with no calcium added, indicating that sulfide is not precipitated

with phosphorus during calcium coagulation. However, there is a small amount of sulfide removal that occurs during the bench-scale coagulation-flocculation-sedimentation process. IC analysis showed similar concentrations of sulfate before and after calcium addition. This suggests that the sulfide removed did not completely oxidize to sulfate, but it could have oxidized to form sulfur, which is an intermediate that would precipitate out (Zwain et al., 2020). Another possibility is volatilization to hydrogen sulfide gas, which would still happen relatively easily at this pH, despite some of the dissolved hydrogen sulfide forming bisulfide, HS^-, given its pKa of 7.05 (Zwain et al., 2020).

Without precipitation, additional downstream processing to remove this residual dissolved hydrogen sulfide from the permeate. One option is to use air sparging to increase volatilization to hydrogen sulfide gas. The challenges with this method are the cost of pumping air into the permeate, as well as the need to monitor the hydrogen sulfide gas levels for safety of those operating the plant. Preliminary results showed a decrease from 30 mg/L S to less than 1 mg/L S after 15 minutes of sparging with air at 1 standard cubic feet per minute (scfm). Other options include additional polishing of the water in and engineered constructed wetland prior to reuse, and additional sulfide removal during ammonia sequestration by zeolite ion exchange.

3.3.4 Calcium Residual and Finished Water Hardness

The residual calcium concentration for each Ca/P ratio of calcium oxide addition tested is displayed below in **Table 3.3**. It should be noted that the calcium residual is larger than the calcium dose added for the 1/1 ratio because there is calcium already present in the synthetic swine permeate. The high calcium residual creates hardness in the effluent of over 200 mg/L as $CaCO_3$ for each concentration and as high as 800 mg/L as $CaCO_3$, classifying it as very hard and significantly higher than Manhattan, Kansas drinking water, which ranges from 80 to 160 mg/L

$CaCO_3$ (Water Research Center, 2020; City of Manhattan). However, hard water does not have reported health impacts on humans or aquatic life (Adey & Loveland, 2007).

Table 3.4. Calcium residual and hardness of permeate after precipitation process

Ca/P ratio	Calcium Oxide added (mg/L Ca)	Ca residual (mg/L Ca)	Hardness (mg/L $CaCO_3$)
1/1	64.71	85.78	214.45
2/1	129.42	101.94	254.85
3/1	199.93	150.05	375.12
4/1	258.83	188.89	472.24
5/1	323.54	246.97	617.42
6/1	388.25	267.06	667.65
7/1	452.95	272.49	681.22
8/1	517.65	325.48	813.69

3.3.5 Future Work

It is important to consider that these results represent phosphorus removal from chemical addition in synthetic swine waste. Future work will need to be done to optimize the quicklime coagulant dose for real swine waste treated through the AnMBR and demonstrate continuous operation of a CFS system with calcium addition and controlled pH.

3.4 References

Adey, W. H., & Loveland, K. (2007). CHAPTER 4 - Water Composition: Management of Salinity, Hardness, and Evaporation. In W. H. Adey & K. Loveland (Eds.), *Dynamic Aquaria (Third Edition)* (pp. 61–74). Academic Press. https://doi.org/10.1016/B978-0-12-370641-6.50013-3

City of Manhattan. Water Division. https://cityofmhk.com/Faq.aspx?QID=35

Damodara Kannan, A., Evans, P., & Parameswaran, P. (2020). Long-term microbial community dynamics in a pilot-scale gas sparged anaerobic membrane bioreactor treating municipal wastewater under seasonal variations. *Bioresource Technology*, *310*, 123425–123425. https://doi.org/10.1016/j.biortech.2020.123425

Fien Degryse, Roslyn Baird, Rodrigo C da Silva, & Mike J McLaughlin. (2017). Dissolution rate and agronomic effectiveness of struvite fertilizers—Effect of soil pH, granulation and base excess. *Plant and Soil*, *410*(1/2), 139–152. https://doi.org/10.1007/s11104-016-2990-2

Huang, H., Xiao, D., Liu, J., Hou, L., & Ding, L. (2015). Recovery and removal of nutrients from swine wastewater by using a novel integrated reactor for struvite decomposition and recycling. *Scientific Reports*, *5*(1), 10183. https://doi.org/10.1038/srep10183

Lei, Y., Song, B., van der Weijden, R. D., Saakes, M., & Buisman, C. J. N. (2017). Electrochemical Induced Calcium Phosphate Precipitation: Importance of Local pH. *Environmental Science & Technology*, *51*(19), 11156–11164. https://doi.org/10.1021/acs.est.7b03909

Lim, K., Evans, P. J., & Parameswaran, P. (2019). Long-Term Performance of a Pilot-Scale Gas-Sparged Anaerobic Membrane Bioreactor under Ambient Temperatures for Holistic Wastewater Treatment. *Environmental Science & Technology*, *53*(13), 7347–7354. https://doi.org/10.1021/acs.est.8b06198

Manure Manager. (1999). Benefits Abound.

Raby, K., Avalos Ramirez, A., & Heitz, M. (2013). Elimination of nitrogen present in swine manure using a high-efficiency biotrickling filter. *Environmental Technology*, *34*(7), 813–824. https://doi.org/10.1080/09593330.2012.720615

Raynaud, S., Champion, E., Bernache-Assollant, D., & Thomas, P. (2002). Calcium phosphate apatites with variable Ca/P atomic ratio I. Synthesis, characterisation and thermal stability of powders. *Biomaterials*, *23*(4), 1065–1072. https://doi.org/10.1016/S0142-9612(01)00218-6

Tran, A. T. K., Zhang, Y., De Corte, D., Hannes, J.-B., Ye, W., Mondal, P., Jullok, N., Meesschaert, B., Pinoy, L., & Van der Bruggen, B. (2014). P-recovery as calcium phosphate from wastewater using an integrated selectrodialysis/crystallization process. *Journal of Cleaner Production*, *77*, 140–151. https://doi.org/10.1016/j.jclepro.2014.01.069

Wang, L., & Nancollas, G. H. (2008). Calcium Orthophosphates: Crystallization and Dissolution. *Chemical Reviews*, *108*(11), 4628–4669. https://doi.org/10.1021/cr0782574

Water Research Center. (2020). Hard Water Hardness Calcium Magnesium Water Corrosion Mineral Scale. https://water-research.net/index.php/water-treatment/tools/hard-water-hardness Accessed 27 April 2021.

Zwain, H. M., Nile, B. K., Faris, A. M., Vakili, M., & Dahlan, I. (2020). Modelling of hydrogen sulfide fate and emissions in extended aeration sewage treatment plant using TOXCHEM simulations. *Scientific Reports*, *10*(1), 22209. https://doi.org/10.1038/s41598-020-79395-8

Chapter 4 - Microbial Electrochemical Systems for Nutrient Recovery

4.1 Introduction

Microbial electrochemical systems (MES) are an emerging environmental biotechnology with great potential for resource recovery, but there has been limited work on using these systems for nutrient recovery. One advantage of these systems for nutrient recovery is their ability to capture ammonium and phosphate from wastewater at low levels, using electric current to drive them into concentrated solutions (Ge et al., 2017; Li et al., 2020). These concentrated solutions are then more efficient for further nutrient capture processes, such as ammonia stripping and chemical phosphorus precipitation (Ge et al., 2017; Li et al., 2020). Precipitation of struvite using microbial fuel cells has been demonstrated previously in MFC and MEC setups (Ichihashi & Hirooka, 2012; Merino-Jimenez et al., 2017), but calcium phosphate and iron phosphate are other options to consider with this setup (Li et al., 2020). Electrocoagulation could also be paired with the MES to precipitate out phosphate with iron from an electrode (Emamjomeh & Sivakumar, 2009).

As described in Chapter 2, calcium phosphate precipitation reduces the phosphate levels in the effluent to 3-15 mg/L P. This is still above the 1.5 mg/L standard proposed by the Kansas Surface Water Nutrient Reduction Plan (Kansas Department of Health and Environment, 2014), which could lead to eutrophication and harmful algal blooms if not treated further. Therefore, MES is proposed as a paired treatment of the AnMBR permeate for further nutrient polishing due to the high loads in swine wastewater.

The first step before evaluating nutrient capture is to understand how the electron donor substrate in wastewater impacts the efficiency of the MES and the coulombic recovery. Coulombic

efficiency measures how much of the electrons from the substrate are converted to current. This is critical because the MES will need to consume wastewater to produce current and drive the nutrient removal. This study evaluates the fate of the electrons from two electron donors, acetate and glucose, to understand how the MES will respond to a more complex substrate as occurs in municipal and swine wastewater. Previous work has shown that acetate-fed reactors have coulombic efficiencies exceeding 70%, while glucose-fed reactors have coulombic efficiencies between 40-60%, but the long-term effects on the efficiencies and the current densities for reactors with these substrates were not evaluated (Freguia et al., 2007; Lee et al., 2008; Torres et al., 2007).

4.2 Materials and Methods

These experiments set up the MFCs as MECs to prevent oxygen diffusion that could inhibit microbial activity (Torres et al., 2009) and to efficiently select for the anode respiring bacteria. Two H-type reactors were used in the experiment, each containing an anode and a cathode compartment separated by an anion exchange membrane (AEM). The two compartments each held a volume of 585 mL. The anode compartment contained two rectangular electrodes in the anode, with a total surface area of 32 cm^2, and the cathode compartment contained one 16 cm^2 rectangular electrode. The anode was maintained at a potential of -301 mV by an Ag/AgCl reference electrode. The reactors were kept in a temperature-controlled environment to maintain 30^o C conditions, while the anode was mixed at a rate of 100 rpm.

The biofilm in each of the two reactors was established by adding anaerobic sludge obtained from the Salina Wastewater Treatment Plant (Salina, Kansas) to the anode. The sludge was added at a concentration of 1% to a phosphate buffer media containing the following composition per liter: 12.04 g Na_2HPO_4, 2.06 g KH_2PO_4, and 0.41 g NH_4Cl; 10 mL of a 1 L trace mineral media

containing 0.5 g EDTA, 0.082 g $CoCl_2*6H_2O$, 0.114 g $CaCl_2*2H_2O$, 0.01 g H_3BO_3, 0.02 g $Na_2MoO_4*2H_2O$, 0.001 g Na_2SeO_3, 0.01 g $Na_2WO_4*2H_2O$, 0.02 g $NiCl_2*6H_2O$, 1.16 g $MgCl_2$, 0.59 g $MnCl_2*4H_2O$, 0.05 g $ZnCl_2$, 0.01 g $CuSO_4*5H_2O$, and 0.01 g $AlK(SO_4)_2$; 1 mL of a 4 g/L $Fe(II)Cl_2$ stock solution; 0.5 mL of a 37.2 g/L Na_2S*9H_2O stock solution; (Parameswaran et al., 2009, 2011). Acetate was then added as an electron donor to grow and condition the biofilm. The cathode media was the same as the anode media, without the sludge or acetate, but was adjusted to a pH of 11.5 using sodium hydroxide. Once the biofilm began to grow on the anode electrodes, the media was replaced with the same composition described above, minus the sludge, and this was iterated until the reactor produced current densities of 5-8 A/m^2.

Three successive trials were conducted in the two reactors, one acetate-fed, and one glucose fed. Each reactor had 100 millielectron equivalents of the respective substrate added to the reactor before the trial began. Additionally, a small volume (1-2 mL) of activated sludge was added to the anode in the glucose-fed reactor to introduce fermenting bacteria to the reactor, since the substrate was a prepared media and not a wastewater stream that would contain its own fermenting microbial community. This was necessary as the biofilm ARB community was enriched for acetate consumption, so the glucose would need to be fermented for current to be produced.

The current production from the reactors was continuously measured using a multichannel potentiostat. The electron donor concentrations were quantified by high performance liquid chromatograph (HPLC) analysis (Shimadzu LC-20AT, USA) using an Aminex HPX-87H column (Bio-Rad Laboratories, USA) to separate the organic acids and sugars which then were detected by a photo diode array and refractive index detectors. Gas production from the anode was measured using a Gas Chromatograph (GC) equipped with a Thermal Conductivity Detector (TCD).

Trials of the acetate-fed and glucose-fed reactors were conducted simultaneously until the current densities reached 0 A/m^2 or the current density had been stable for multiple days.

4.3 Electron Balance Studies

Current densities of the acetate-fed and glucose-fed MEC reactors were measured for 10 days for each of the three trials. As shown in **Figure 4.1** below, the acetate-fed reactors produced higher peak current densities than the glucose fed-reactors by 3-4 A/m^2. The peak current densities of the glucose-fed reactor are also delayed, as the ARB are acetate-enriched and require fermentation of the glucose before current production can begin. Fermentation continues to provide a limited supply of acetate for the entire 10 days, allowing the glucose-fed reactor to retain current densities of 0.5-1 A/m^2, while the acetate-fed reactor reaches 0 A/m^2 after around 6 days.

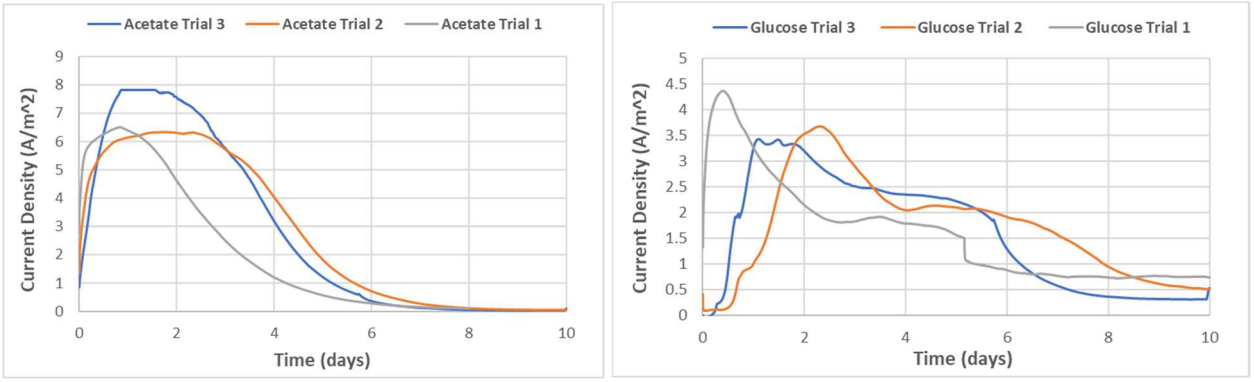

a) b)

Figure 4.1. Current density from batch operation of a) acetate fed-reactor and b) glucose-fed reactor.

To further explore the differences in current production between the two reactors, the fate of the electrons from the substrate and the resulting coulombic recovery needed to be established. The coulombic efficiencies for the reactors were calculated using Equation 1:

(1) $$CE = 100\% \times \frac{I_{cum} \times F}{V \times \Delta COD}$$

in which I_{cum} = the cumulative current over the batch-operating period, V = the anode's volume (L), F is the Faraday constant (96485 C/e^- eq), and ΔCOD is the change in chemical oxygen demand in the electron donor (acetate or glucose). As shown in **Figure 4.2**, the acetate-fed reactor had coulombic efficiencies of 64-80% and the glucose-fed reactor had coulombic efficiencies of 45-50%.

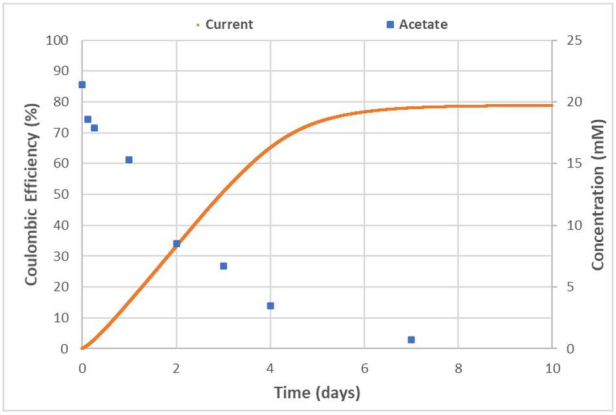

a) Acetate Trial 2

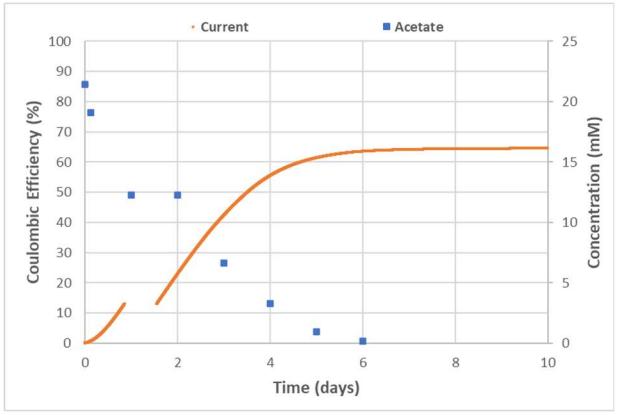

b) Acetate Trial 3

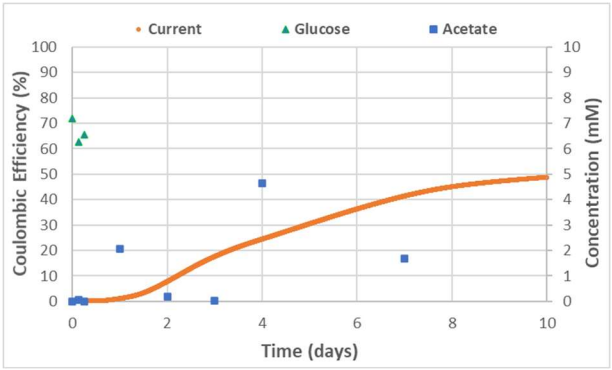

c) Glucose Trial 2

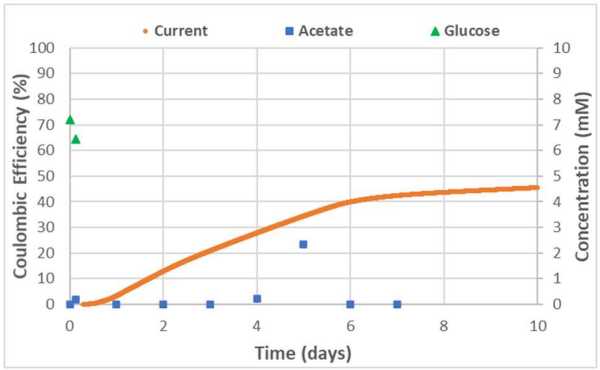

d) Glucose Trial 3

Figure 4.2. Electron balance for acetate-fed (a and b) and glucose-fed (c and d) reactors corresponding to trials 2 and 3 from Figure *4*.1 comparing current density.

The differences in coulombic efficiency are due to additional electron sinks in the glucose-fed reactor, driven by the need for fermentation. These sinks include intermediate fermentation products, along with methane. These volatile fatty acid intermediate products include propionate, butyrate, lactate, iso-butyrate, valerate, and iso-valerate. HPLC analysis did not show these as

present in the glucose-fed reactors, but most likely they were present at values below the detection limit, as these are products of the fermentation that had to take place for current to be produced. Methane was determined to be the largest sink that diverted electrons from current. As shown in **Figure 4.3** below, the methane in the anode headspace of the glucose-fed reactor had a concentration over five times higher than that of the acetate-fed reactor, based on data from the Gas Chromatograph. This is a result of accumulated hydrogen from fermentation of glucose, which is then converted to methane by hydrogenotrophic methanogens (Parameswaran et al., 2009, 2011).

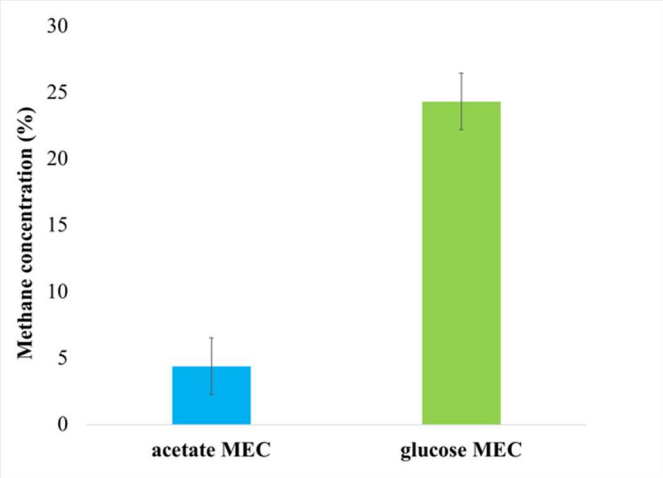

Figure 4.3. Methane concentration measured in headspace of the acetate and glucose-fed reactors.

As methane is the largest electron sink, reducing methane production should be the highest priority for improving efficiencies and current production in reactors fed by more complex substrates. It has already been demonstrated that adding 2-bromoethane sulfonic acid (BES) to an MEC reactor can inhibit methanogenesis and increase coulombic efficiency (Parameswaran et al., 2009). With methanogenesis inhibited, homo-acetogens can then convert the accumulated hydrogen to acetate, which creates syntropy with ARB that then use the acetate for further current production (Parameswaran et al., 2009, 2011).

4.4 Future Work

After evaluating the electron balance of different substrates and the effect on current production, future work can focus on using the current produced by the MES reactors to recovery nutrients by capacitive deionization. A flat-plate electrode MFC with a cathode exposed to air will be used for these experiments. The reactor will use the swine permeate before or after calcium coagulation to capture remaining phosphorus. Multiple methods can be evaluated to precipitate out the phosphorus using this reactor. One option is to utilize calcium precipitation for this system as well by using current produced from the MFC to concentrate both the calcium and the phosphorus in the cathode using multiple alternatingly charged (anion or cation) membranes (Lei et al., 2017; Tran et al., 2014). Other options involve using electrocoagulation with iron or magnesium electrodes to induce vivianite or struvite precipitation, respectively. Struvite precipitation would produce a more readily commercial product and has the advantage of also removing additional ammonia in the permeate. This reactor should also be evaluated with municipal wastewater, where it can concentrate the more dilute nutrient concentrations in this stream.

These MES systems will need to be scaled up to the pilot system to perform these experiments. The economic feasibility of microbial electrochemical systems and electrocoagulation for full-scale wastewater treatment plants will also need to be evaluated.

4.5 References

Emamjomeh, Mohammad. M., & Sivakumar, Muttucumaru. (2009). Review of pollutants removed by electrocoagulation and electrocoagulation/flotation processes. *Journal of Environmental Management*, *90*(5), 1663–1679. https://doi.org/10.1016/j.jenvman.2008.12.011

Freguia, S., Rabaey, K., Yuan, Z., & Keller, J. (2007). Electron and Carbon Balances in Microbial Fuel Cells Reveal Temporary Bacterial Storage Behavior During Electricity Generation. *Environmental Science & Technology*, *41*(8), 2915–2921. https://doi.org/10.1021/es062611i

Ge, Z., Chen, X., & Ren, Z. (2017). Capacitive Deionization for Nutrient Recovery from Wastewater with Disinfection Capability. *Environ. Sci.: Water Res. Technol.*, *4*. https://doi.org/10.1039/C7EW00350A

Ichihashi, O., & Hirooka, K. (2012). Removal and recovery of phosphorus as struvite from swine wastewater using microbial fuel cell. *Bioresource Technology*, *114*, 303–307. https://doi.org/10.1016/j.biortech.2012.02.124

Lee, H.-S., Parameswaran, P., Kato-Marcus, A., Torres, C. I., & Rittmann, B. E. (2008). Evaluation of energy-conversion efficiencies in microbial fuel cells (MFCs) utilizing fermentable and non-fermentable substrates. *Water Research (Oxford)*, *42*(6), 1501–1510. https://doi.org/10.1016/j.watres.2007.10.036

Lei, Y., Song, B., van der Weijden, R. D., Saakes, M., & Buisman, C. J. N. (2017). Electrochemical Induced Calcium Phosphate Precipitation: Importance of Local pH. *Environmental Science & Technology*, *51*(19), 11156–11164. https://doi.org/10.1021/acs.est.7b03909

Li, N., Wan, Y., & Wang, X. (2020). Nutrient conversion and recovery from wastewater using electroactive bacteria. *Science of The Total Environment*, *706*, 135690. https://doi.org/10.1016/j.scitotenv.2019.135690

Merino-Jimenez, I., Celorrio, V., Fermin, D. J., Greenman, J., & Ieropoulos, I. (2017). Enhanced MFC power production and struvite recovery by the addition of sea salts to urine. *Water Research*, *109*, 46–53. https://doi.org/10.1016/j.watres.2016.11.017

Parameswaran, P., Torres, C. I., Lee, H.-S., Krajmalnik-Brown, R., & Rittmann, B. E. (2009). Syntrophic interactions among anode respiring bacteria (ARB) and Non-ARB in a biofilm anode: Electron balances. *Biotechnology and Bioengineering*, *103*(3), 513–523. https://doi.org/10.1002/bit.22267

Parameswaran, P., Torres, C. I., Lee, H.-S., Rittmann, B. E., & Krajmalnik-Brown, R. (2011). Hydrogen consumption in microbial electrochemical systems (MXCs): The role of homo-acetogenic bacteria. *Bioresource Technology*, *102*(1), 263–271. https://doi.org/10.1016/j.biortech.2010.03.133

Torres, C. I., Kato Marcus, A., & Rittmann, B. E. (2007). Kinetics of consumption of fermentation products by anode-respiring bacteria. *Applied Microbiology and Biotechnology*, *77*(3), 689–697. https://doi.org/10.1007/s00253-007-1198-z

Torres, C. I., Krajmalnik-Brown, R., Parameswaran, P., Marcus, A. K., Wanger, G., Gorby, Y. A., & Rittmann, B. E. (2009). Selecting Anode-Respiring Bacteria Based on Anode Potential: Phylogenetic, Electrochemical, and Microscopic Characterization. *Environmental Science & Technology*, *43*(24), 9519–9524. https://doi.org/10.1021/es902165y

Tran, A. T. K., Zhang, Y., De Corte, D., Hannes, J.-B., Ye, W., Mondal, P., Jullok, N., Meesschaert, B., Pinoy, L., & Van der Bruggen, B. (2014). P-recovery as calcium phosphate from wastewater using an integrated selectrodialysis/crystallization process. *Journal of Cleaner Production*, *77*, 140–151. https://doi.org/10.1016/j.jclepro.2014.01.069